In Vitro Characterization of AtsB, a Radical SAM Formylglycine-Generating Enzyme That Contains Three [4Fe-4S] Clusters[†]

Tyler L. Grove,[‡] Kyung-Hoon Lee,[§] Jennifer St. Clair,[§] Carsten Krebs,*[,‡,§] and Squire J. Booker*[,‡,§]

Department of Chemistry and Department of Biochemistry and Molecular Biology, The Pennsylvania State University, University Park, Pennsylvania 16802

Received March 13, 2008; Revised Manuscript Received May 5, 2008

ABSTRACT: Sulfatases catalyze the cleavage of a variety of cellular sulfate esters via a novel mechanism that requires the action of a protein-derived formylglycine cofactor. Formation of the cofactor is catalyzed by an accessory protein and involves the two-electron oxidation of a specific cysteinyl or seryl residue on the relevant sulfatase. Although some sulfatases undergo maturation via mechanisms in which oxygen serves as an electron acceptor, AtsB, the maturase from *Klebsiella pneumoniae*, catalyzes the oxidation of Ser72 on AtsA, its cognate sulfatase, via an oxygen-independent mechanism. Moreover, it does not make use of pyridine or flavin nucleotide cofactors as direct electron acceptors. In fact, AtsB has been shown to be a member of the radical *S*-adenosylmethionine superfamily of proteins, suggesting that it catalyzes this oxidation via an intermediate 5′-deoxyadenosyl 5′-radical that is generated by a reductive cleavage of *S*-adenosyl-L-methionine. In contrast to AtsA, very little in vitro characterization of AtsB has been conducted. Herein we show that coexpression of the *K. pneumoniae atsB* gene with a plasmid that encodes genes that are known to be involved in iron−sulfur cluster biosynthesis yields soluble protein that can be characterized in vitro. The as-isolated protein contained 8.7 ± 0.4 irons and 12.2 ± 2.6 sulfides per polypeptide, which existed almost entirely in the $[4Fe\text{-}4S]^{2+}$ configuration, as determined by Mössbauer spectroscopy, suggesting that it contained at least two of these clusters per polypeptide. Reconstitution of the as-isolated protein with additional iron and sulfide indicated the presence of 12.3 ± 0.2 irons and 9.9 ± 0.4 sulfides per polypeptide. Subsequent characterization of the reconstituted protein by Mössbauer spectroscopy indicated the presence of only [4Fe-4S] clusters, suggesting that reconstituted AtsB contains three per polypeptide. Consistent with this stoichiometry, an as-isolated AtsB triple variant containing Cys → Ala substitutions at each of the cysteines in its CX_3CX_2C radical SAM motif contained 7.3 ± 0.1 irons and 7.2 ± 0.2 sulfides per polypeptide while the reconstituted triple variant contained 7.7 ± 0.1 irons and 8.4 ± 0.4 sulfides per polypeptide, indicating that it was unable to incorporate an additional cluster. UV−visible and Mössbauer spectra of both samples indicated the presence of only [4Fe-4S] clusters. AtsB was capable of catalyzing multiple turnovers and exhibited a $V_{max}/[E_T]$ of ∼0.36 min^{-1} for an 18-amino acid peptide substrate using dithionite to supply the requisite electron and a value of ∼0.039 min^{-1} for the same substrate using the physiologically relevant flavodoxin reducing system. Simultaneous quantification of formylglycine and 5′-deoxyadenosine as a function of time indicates an approximate 1:1 stoichiometry. Use of a peptide substrate in which the target serine is changed to cysteine also gives rise to turnover, supporting approximately 4-fold the activity of that observed with the natural substrate.

Sulfatases catalyze the cleavage of a variety of organosulfate esters, resulting in the release of inorganic sulfate and the corresponding alcohol (*1–4*). Three classes of these enzymes are currently recognized and are delineated by the cofactors they employ in catalysis (*5*). Group I enzymes are often termed arylsulfatases, but their substrate profile extends beyond that designation since they catalyze sulfate hydrolysis from myriad sulfated compounds. In addition to a calcium or magnesium ion, they require a C_α-formylglycine (2-amino-3-oxopropionic acid) cofactor, which is generated via a cotranslational or post-translational modification of a specific cysteinyl or seryl residue on the enzyme (Scheme 1A) (*6*). Group II enzymes catalyze sulfate release via an oxidative mechanism, employing Fe(II) as a cofactor, and α-ketoglutarate and molecular oxygen as cosubstrates. Concomitant with sulfate release, 1 equiv each of carbon dioxide, succinate, and an aldehyde or ketone is produced (*5, 7*). Group III enzymes constitute the least characterized sulfatase designation. They employ a dinuclear zinc center to activate water for nucleophilic attack on the sulfated substrate in a fashion analogous to that of members of the metallo-β-lactamase family (*8*).

[†] This work was supported by NIH Grant GM-63847 (S.J.B.), the Dreyfus Foundation (Teacher Scholar Award to C.K.), and the Beckman Foundation (Young Investigator Award to C.K.).

* To whom correspondence should be addressed. S.J.B.: 104 Chemistry Building, The Pennsylvania State University, University Park, PA 16802; phone, (814) 865-8793; fax, (814) 865-2927; e-mail, sjb14@psu.edu. C.K.: 104 Chemistry Building, The Pennsylvania State University, University Park, PA 16802; phone, (814) 865-6089; fax, (814) 865-2927; e-mail, ckrebs@psu.edu.

[‡] Department of Chemistry.

[§] Department of Biochemistry and Molecular Biology.

10.1021/bi8004297 CCC: $40.75
Published on Web 06/18/2008

Scheme 1: AtsB-Dependent Oxidation of Ser72 of AtsA from *Klebsiella pneumoniae* To Afford the FGly Cofactor[a]

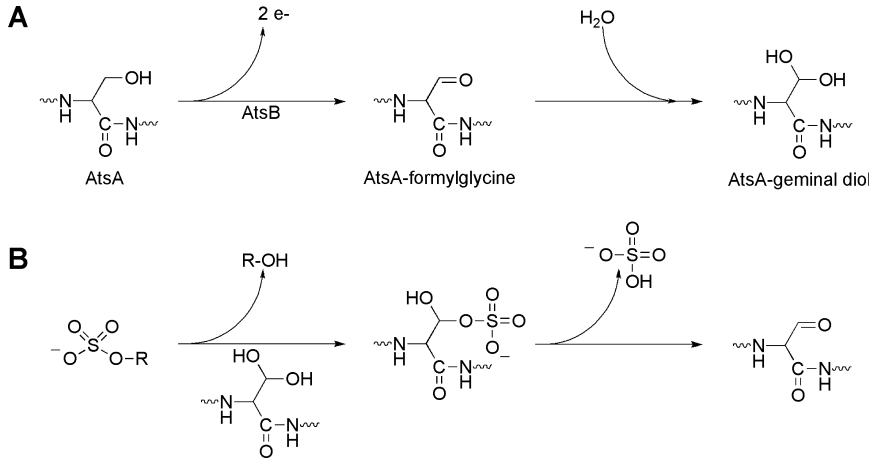

[a] Also shown is the subsequent hydration of the aldehyde to give the geminal diol, which is the active form of the cofactor (A). This is the proposed mechanism of action of the FGly cofactor. The first step involves a nucleophilic attack on the sulfate group by the geminal diol form of the FGly cofactor with concomitant modification of the FGly cofactor and release of the corresponding alcohol. The second step is an internal elimination, which results in regeneration of the FGly cofactor (B).

Group I sulfatases have been the most extensively studied and characterized (*1–4, 9–11*). Although mostly eukaryotic, these enzymes are also found in archaea and bacteria. In bacteria, sulfatase genes are often expressed under conditions of sulfate starvation, and the gene products are believed to play a role in sulfate scavenging or the metabolism of sulfated compounds (*12, 13*). In eukaryotes, sulfatases catalyze key steps in the breakdown of sulfate-containing compounds, such as the hydrolysis of sulfate ester linkages in glycosaminoglycans, steroids, lipids, and various other molecules. Catalytic deficiencies in eight identified sulfatases lead to severe metabolic disorders, derived from their inability, or weakened ability, to hydrolyze specific sulfate-containing metabolites (*3*). A rare autosomal recessive disease, multiple-sulfatase deficiency (MSD[1]), is a pleiotropic condition in which the essential formylglycine (FGly) cofactor is not formed on most, if not all, sulfatases (*6, 14, 15*).

The FGly modification is found in a signature sequence (**C/S**-X-P/A-S/X-R-X-X-X-L/X-T/X-G/X-R/X) that is highly conserved from prokaryotes to eukaryotes, wherein the initial cysteine or serine amino acid (shown in bold type) is that which is modified (*6, 16*). All eukaryotic group I sulfatases contain a FGly cofactor derived from a cysteinyl residue, as do many bacterial sulfatases; however, some bacterial sulfatases also contain FGly cofactors that are derived from a seryl residue, giving rise to the classification Ser-type or Cys-type sulfatase (*2, 17, 18*). The manner in which the cofactor is used in organosulfate hydrolysis is novel. Crystallographic studies of human arylsulfatase A (HARSA) (*19*), as well as an arylsulfatase from *Pseudomonas aeruginosa* (*9*), show that the FGly cofactor exists in its hydrated form as a geminal diol (Scheme 1A). It is proposed that one of the hydroxyls of the hydrated cofactor performs a nucleophilic attack on the sulfur atom of the organosulfate substrate with concomitant transfer of the sulfate group to the cofactor and release of the corresponding alcohol. Deprotonation of the remaining hydroxyl group of the cofactor allows for elimination of inorganic sulfate and regeneration of the cofactor. Subsequent hydration of the cofactor re-establishes its active form (Scheme 1B) (*4, 9, 19*). Consistent with this mechanism, variants of HARSA and HARSB containing a Ser substitution at the Cys residue that is converted to FGly become irreversibly sulfated at the Ser residue when treated with [^{35}S]-*p*-nitrocatechol sulfate, suggesting that these two variant human sulfatases can perform the nucleophilic attack on the organosulfate substrate but cannot eliminate the adduct (*20*). Note that, as opposed to some bacterial sulfatases, eukaryotic sulfatase maturation proteins cannot convert Ser residues into FGly.

Two mechanisms are currently recognized for generation of the FGly cofactor. In higher eukaryotes, FGly generation takes place in the endoplasmic reticulum and is catalyzed by sulfatase modifying factor 1 (SUMF1) (*14, 15*). This protein is the product of the *SUMF1* gene, which is the locus for mutations that give rise to MSD. The detailed mechanism by which this enzyme catalyzes its reaction has not been elucidated; however, SUMF1 contains a redox-active disulfide bond but no redox-active metals or other cofactors and is reported to require both dioxygen and reducing equivalents for catalysis. The intermediacy of a cysteine sulfenic acid on the substrate has been proposed (*10*).

A second mechanism for FGly generation is found almost exclusively in prokaryotes and does not involve dioxygen. The prototype of this FGly-generating system is the enzyme AtsB from *Klebsiella pneumoniae*, which catalyzes FGly formation on its cognate protein AtsA, a Ser-type sulfatase (*21–23*). This sulfatase, like most, if not all, Ser-type sulfatases,

[1] Abbreviations: aa, amino acid; AI, as-isolated; BDE, bond dissociation energy; BME, β-mercaptoethanol; BS, biotin synthase; 5′-dA, 5′-deoxyadenosine; 5′-dA$^{\bullet}$, 5′-deoxyadenosyl radical; DTT, dithiothreitol; EPR, electron paramagnetic resonance; Fe/S, iron−sulfur; FGE, formylglycine-generating enzyme; FGly, formylglycine; Flv, flavodoxin; Flx, flavodoxin reductase; HemN, coproporphyrinogen III oxidase; HEPES, *N*-(2-hydroxyethyl)piperazine-*N*′-2-ethanesulfonic acid; HPLC, high-performance liquid chromatography; IMAC, immobilized metal affinity chromatography; IS, internal standard; LS, lipoyl synthase; MALDI, matrix-assisted laser desorption ionization; MS, mass spectrometry; MSD, multiple-sulfatase deficiency; Ni-NTA, nickel nitrilotriacetic acid; PCR, polymerase chain reaction; RCN, reconstituted; RS, radical SAM; SAM, *S*-adenosyl-L-methionine; SDS−PAGE, sodium dodecyl sulfate−polyacrylamide gel electrophoresis; SUMF1, sulfatase modifying factor 1; WT, wild-type.

contains a periplasmic localization sequence, the removal of which drastically reduces the efficiency of FGly modification in vivo (*2, 22*). AtsB, however, does not harbor a periplasmic localization signal sequence and is believed to act on AtsA either cotranslationally or during translocation into the periplasm. Cys-type sulfatases, by contrast, are believed to be located predominantly in the cytoplasm (*2*).

AtsB is composed of 395 amino acids, and its primary structure predicts a molecular mass of 44237 Da (*24*). Although it was once believed to be a transcriptional regulator of AtsA, the absence of clear DNA binding domains, as determined by bioinformatics analysis, cast doubt on this role in sulfatase function (*2*). In fact, AtsB contains 13 Cys residues, 10 of which are conserved among known and predicted FGly maturation proteins within this class (*2, 24*). Three of the cysteines are organized in a CX_3CX_2C motif, which is the predominant signature sequence that denotes a superfamily of enzymes, the radical SAM (RS) superfamily, that use *S*-adenosyl-L-methionine (SAM) as a precursor to a 5′-deoxyadenosyl 5′-radical (5′-dA•) (*25*). The 5′-dA• initiates catalysis on an appropriate substrate by abstracting a key hydrogen atom, affording 5′-deoxyadenosine (5′-dA) and a substrate-derived organic radical intermediate. The generation of the 5′-dA• from SAM requires the input of one electron, which emerges from a reduced [4Fe-4S] cluster ($[4Fe\text{-}4S]^+$) that is ligated to the protein by the three cysteines within the hallmark CX_3CX_2C motif (*26–29*). The one iron atom of the cluster not ligated by a protein-derived residue binds in contact with the α-amino and α-carboxylate groups of SAM, allowing for close spatial arrangement and optimal geometry for electron transfer into the sulfonium group (*30–37*).

Like many iron−sulfur (Fe/S) proteins, RS proteins tend to be exquisitely sensitive to oxygen and upon heterologous overproduction often assemble into inclusion bodies, especially when incorporation of the cluster lags well behind production of the polypeptide scaffold. AtsB is no exception; these tendencies have hampered its in vitro characterization. However, characterization of AtsB in vivo or in cell lysates has confirmed its identity as a RS protein (*23*). AtsB was shown to associate with a GST-fused AtsA fragment, and this association was stimulated in the presence of SAM. Moreover, AtsB catalyzed FGly formation on the GST-fused AtsA fragment only in the presence of SAM, although the efficiency of conversion was calculated to be ∼10% (*23*). Herein, we describe the first purification and in vitro characterization of AtsB from *K. pneumoniae*. The enzyme is shown by analytical methods and Mössbauer spectroscopy to contain three [4Fe-4S] clusters per polypeptide as predicted by an early bioinformatics study (*2*). In addition, AtsB is shown to catalyze formation of 5′-dA and FGly in a 1:1 ratio using an 18-amino acid (aa) peptide substrate. Substitution of the target Ser residue in the peptide substrate with Ala abolished formation of both 5′-dA and FGly; however, substitution of the Ser residue with Cys gave rise to a peptide substrate that was converted to product with a faster $V_{max}/[E_T]$. Finally, a working model for this interesting transformation that is consistent with the data described is presented.

MATERIALS AND METHODS

Materials. All DNA-modifying enzymes and reagents were purchased from New England Biolabs (Beverly, MA), as were DeepVent polymerase and its associated 10× buffer. Oligonucleotide primers were obtained from Integrated DNA Technologies (Coralville, IA). *Escherichia coli* BL21(DE3) and expression vector pET-28a were purchased from Novagen (Madison, WI). Phenylhydrazine, 5′-deoxyadenosine (5′-dA), sodium sulfide (nonahydrate), dithiothreitol (DTT), reduced nicotinamide adenine dinucleotide phosphate (NADPH), β-mercaptoethanol, L-tryptophan, and L-(+)-arabinose were purchased from Sigma-Aldrich Chemicals (St. Louis, MO) and used as is. Bovine serum albumin (BSA) standard (2 mg/mL) and the Bradford reagent for protein concentration determination were purchased from Pierce (Rockford, IL). *K. pneumoniae* genomic DNA (ATCC 700721D) was obtained from the American Type Culture Collection (Manassas, VA). Nickel nitrilotriacetic acid (Ni-NTA) resin was purchased from Qiagen (Valencia, CA), while Talon metal affinity resin was purchased from Clontech (Moutain View, CA). Sephadex G-25 resin and NICK and NAP prepoured gel filtration columns were purchased from GE Biosciences (Piscataway, NJ). All other buffers and chemicals were of the highest grade available.

S,*S*-Adenosyl-L-methionine (SAM) was synthesized enzymatically and purified as described previously (*38*). *E. coli* flavodoxin (Flv) and flavodoxin reductase (Flx) were purified from *E. coli* BL21(DE3) containing plasmids pTYB1-Flv and pTYB1-Flx, which harbor the genes for *E. coli* Flv and Flx, respectively, cloned into the *Nde*I and *Sap*I sites of plasmid pTYB1 (New England Biolabs). This construct affords production of Flv and Flx as intein fusions, which undergo splicing in the presence of DTT such that both target proteins are produced in their native forms.

General Methods. High-performance liquid chromatography (HPLC) was conducted on an Agilent (Foster City, CA) 1100 system that was fitted with an autosampler for sample injection and a variable-wavelength detector. The system was operated with the associated ChemStation software package, which was also used for data collection and analysis. Iron and sulfide analyses were performed by the methods of Beinert as previously described (*39–41*). Sonic disruption of *E. coli* cells was carried out with a 550 sonic dismembrator from Fisher Scientific (Pittsburgh, PA) using a horn containing a $^1/_2$ in. tip. The cable connecting the horn to the power supply was threaded through a port in a Coy Laboratory Products, Inc. (Grass Lake, MI) anaerobic chamber to allow sonic disruption to be performed under an oxygen-free atmosphere. DNA sequencing was conducted at The Pennsylvania State University Nucleic Acids Facility (University Park, PA), and peptide synthesis was performed at The Pennsylvania State University College of Medicine Core Facility (Hershey, PA).

Spectroscopic Methods. UV−visible spectra were recorded on a Cary 300 spectrometer (Varian, Walnut Creek, CA), employing the associated WinUV software package for operating the instrument and manipulating the data. Mössbauer spectra were recorded on a spectrometer from WEB Research (Edina, MN), which was equipped with an SVT-400 cryostat from Janis Research Co. (Wilmington, MA). Spectra were collected in constant acceleration mode in transmission geometry. Isomer shifts are quoted relative to the centroid of α-Fe at room temperature. Spectra were analyzed with the program WMOSS from WEB Research. Matrix-assisted laser desorption ionization (MALDI) mass

spectrometry was performed on a MALDI micro MX instrument from Waters Corp. (Milford, MA). Spectra were combined and refined with the assistance of the associated MassLynx software package.

Construction of the atsB Expression Vector. The *atsB* gene was amplified from *K. pneumoniae* genomic DNA using polymerase chain reaction (PCR) technology. The forward amplification primer (5′-CGC CGC CCC CAT ATG CTG AAT GCC CTG CGC CAG CAG C-3′) included an *Nde*I restriction site (underlined) flanked by a 9 bp GC clamp and the first 31 bases of the *atsB* gene. The reverse primer (5′-CGC CGC CCC GAA TTC CTA CGC AGT ATG CGC AGT CCC AAC AAA CGC-3′) contained an *Eco*RI restriction site (underlined) flanked by a 9 bp GC clamp and the last 30 bases of the *atsB* gene, including the stop codon. The PCR was performed with a Stratagene (La Jolla, CA) Robocycler thermocycler as described previously (*42*). The product was isolated and digested with *Nde*I and *Eco*RI and ligated into similarly digested expression vector pET-28a by standard procedures (*43*). The correct construct was verified by DNA sequencing and designated pAtsBWt.

Construction of the AtsB C35A/C39A/C42A Triple Variant. The gene for the AtsB C35A/C39A/C42A triple variant was constructed using the Stratagene QuikChange II site-directed mutagenesis kit according to the manufacturer's specifications, and as described previously (*42, 44*). The following modifications were implemented to allow three mutations to be constructed in one PCR. The forward primer (5′-CCG TTT CAT ATT CTG ATG AAG CCG ATT GGC CCC GCC **GCC AAT CTC GCC GCC CGC TAT GCC**-3′) contained 60 bases, the last 24 of which were complementary to the last 24 bases of the reverse primer (5′-CAT CTT GTT GAC CGG CGT TTC GTC CTG CGG GTA ATA **GGC ATA GCG GGC GGC GAG ATT GGC**-3′) (shown in bold type; base changes are underlined). These primers were added to a typical QuikChange II reaction mixture to a final concentration of 20 μM, and 10 cycles of the following program were initiated: 95 °C for 1 min, 50 °C for 1.5 min, and 72 °C for 1 min. This initial thermocycling reaction allows creation of 96-base primers from the initial PCR, deriving from overlap extension of the forward and reverse primers after they anneal. The template plasmid, pAtsBWt (100 ng), was then added to the reaction mixture, and 15 cycles of the following program were initiated: 95 °C for 1 min, 55 °C for 1.5 min, and 72 °C for 10 min. Upon completion, the reaction mixture was incubated for 10 min at 72 °C before being cooled to 4 °C. Subsequent to this step, the procedure followed the manufacturer's specifications. Mutations were verified by DNA sequencing, and the resulting plasmid was designated pAtsBMut1.

Expression of the atsB Gene and Production and Purification of AtsB. For expression of the *atsB* gene, plasmid pAtsBWt was transformed into *E. coli* BL21(DE3)/pDB1282 by standard methods (*43*). A single colony was used to inoculate 200 mL of M9 minimal medium containing 100 μg/mL ampicillin and 50 μg/mL kanamycin. The culture was allowed to grow to late-log phase, after which 20 mL portions were used to inoculate four 6 L flasks, each of which contained 4 L of the same medium. The cultures were allowed to grow with moderate shaking (180 rpm) to an optical density (OD) at 600 nm of 0.3, after which solid L-(+)-arabinose was added to each flask to a final concentration of 0.2% (w/v), while cysteine and ferric chloride were added to final concentrations of 200 and 50 μM, respectively. At an OD_{600} of 0.6, the flasks were cooled to 18 °C before a sterile solution of IPTG was added to each flask to a final concentration of 200 μM. Expression was allowed to take place during a further incubation at 18 °C for 20−23 h, after which the cultures were harvested by centrifugation at 10000*g* for 10 min at 4 °C. Typical yields were 60−65 g of frozen cell paste from 16 L of M9 minimal medium. The frozen cell paste was stored at −80 °C until it was needed for further use.

AtsB was purified by immobilized metal affinity chromatography (IMAC) using Talon metal affinity chromatography medium. All steps were performed inside a Coy Laboratory Products anaerobic chamber under an atmosphere of nitrogen (90%) and hydrogen (10%) gas. The oxygen concentration was monitored with a H_2/O_2 meter (Coy Laboratory Products) that was housed inside the chamber and was maintained below 1 ppm via the use of palladium catalysts (Coy Laboratory Products). All buffers were prepared using distilled and deionized water that was boiled for several hours before introduction into the anaerobic chamber and then allowed to cool while being stirred uncapped for 48 h. They were titrated to their final pH values using an Accumet (AP61) pH meter from Fisher Scientific (Fairlawn, NJ), which was housed inside the anaerobic chamber. All plasticware was autoclaved and introduced inside of the chamber while still hot and allowed to equilibrate with the atmosphere for at least 24 h. Centrifugation was performed outside the anaerobic chamber; however, samples were loaded into airtight centrifuge bottles before they were removed. Concentration by ultrafiltration was conducted inside the anaerobic chamber using an Amicon (Millipore, Billerica, MA) stirred cell that was connected to an argon tank via a port in the chamber. Although the purification was carried out at room temperature, all solutions were kept in ice/water baths, and during protein concentration, the Amicon stirred cell was loosely jacketed with ice packs.

In a typical purification, 30 g of cell paste was resuspended in 150 mL of lysis buffer [50 mM potassium HEPES (pH 7.5), 300 mM KCl, 10 mM BME, and 20 mM imidazole] containing lysozyme and peptide **3** (see below) at final concentrations of 1 mg/mL and 10 μM, respectively. After being stirred at room temperature for 30 min, the solution was placed in an ice/water bath and allowed to cool to ∼4 °C before being subjected to four 1 min bursts of sonic disruption (40% output). Between bursts, the solution was allowed to stir in the ice/water bath for 10 min to re-equilibrate the temperature to ≤8 °C. The lysate was centrifuged for 1 h at 50000*g* and 4 °C, and the resulting supernatant was loaded onto a Talon cobalt affinity column (2.5 cm × 10 cm). The column was washed with 200 mL of lysis buffer and then eluted with 100 mL of elution buffer [50 mM potassium HEPES (pH 7.5), 300 mM KCl, 20% glycerol, 10 mM BME, and 300 mM imidazole]. Fractions that exhibited significant brown color were collected, and peptide **3** (see below) was added to the pooled sample to a final concentration of 50 μM to stabilize the protein. The protein solution was concentrated to ∼3 mL by stirred ultrafiltration using a Millipore YM-3 membrane and exchanged into gel filtration buffer [50 mM potassium HEPES (pH 7.5), 500 mM KCl, 10 mM DTT, and 30% glycerol]

using a Sephadex G-25 column. The brown fractions were pooled and concentrated to ~3 mL. The protein was snap-frozen in liquid nitrogen in 200 μL aliquots and stored at −80 °C. When necessary, reconstitution of the Fe/S clusters of AtsB was carried out as previously described, but in the presence of equimolar concentrations of peptide **3** (*42*).

Amino Acid Analysis of AtsB. Amino acid analysis of AtsB was carried out at the Molecular Structure Facility at the University of California (Davis, CA) as well as the Molecular Biology Core Facility of the Dana Farber Institute (Boston, MA). The protein was exchanged by gel filtration (NICK prepoured column) into 50 mM HEPES buffer (pH 7.5) containing 100 mM NaCl. The eluate was divided into 150 μL fractions, which were lyophilized to dryness using a Savant SpeedVac concentrator (Thermo Scientific, Waltham, MA). One fraction was used to determine the protein concentration by the procedure of Bradford (*45*) before lyophilization. The remaining fractions were shipped for amino acid analysis, which was performed on three different samples.

Quantification of Turnover. Turnover was assessed using four synthetic peptides as substrates: NH_2-Tyr-Tyr-Thr-Ser-Pro-Met-Ser-Ala-Pro-Ala-Arg-Ser-Met-Leu-Leu-Thr-Gly-Asn-COOH (peptide **1**), acetyl-Tyr-Tyr-Thr-Ser-Pro-Met-Ser-Ala-Pro-Ala-Arg-Ser-Met-Leu-Leu-Thr-Gly-Asn-COOH (peptide **2**), NH_2-Tyr-Tyr-Thr-Ser-Pro-Met-Cys-Ala-Pro-Ala-Arg-Ser-Met-Leu-Leu-Thr-Gly-Asn-COOH (peptide **3**), and NH_2-Tyr-Tyr-Thr-Ser-Pro-Met-Ala-Ala-Pro-Ala-Arg-Ser-Met-Leu-Leu-Thr-Gly-Asn-COOH (peptide **4**). Note that the underlined amino acids in each peptide are at the position that undergoes modification to FGly. Assays conducted using sodium dithionite as the reductant contained the following in a final volume of 350 μL: 50 mM HEPES (pH 7.5), 2 mM dithionite, 1 mM peptide substrate, 1 mM SAM, 50 or 100 μM AtsB, and 1 mM L-tryptophan (internal standard). Reactions were initiated by addition of dithionite after incubation of the other components of the assay mixture at 37 °C for 5 min. At designated times, 25 μL aliquots were removed and added to an equal volume of 1 M HCl. Precipitated protein was pelleted by centrifugation, and the resulting supernatant was removed. A 1.5 μL aliquot of the supernatant was mixed with 1.5 μL of α-cyano-4-hydroxycinnamic acid [5 mg/mL in 70% acetonitrile and 30% TFA (0.1%)], and 2 μL of this mixture was spotted onto the MALDI-TOF target plate. Spectra (70−100, 10 scans per spectrum) were acquired in reflector mode with an accelerating voltage of 21 kV, a grid voltage of 65%, and a delay of 500 ns. The resulting data were transformed into *X*,*Y* format and then plotted using Igor Pro (Wavemetrics, Lake Oswego, OR). Assays in which Flv and Flx replaced sodium dithionite contained the same components as described above, except that dithionite was omitted and Flv, Flx, and NADPH were added to final concentrations of 25 μM, 5 μM, and 2 mM, respectively. In addition, the AtsB concentration was increased to 100 μM, and reactions were initiated by addition of SAM.

A second, HPLC-based, method was also developed to quantify the FGly product, the peptide substrate, and 5′-dA. Activity assays were conducted as described above, except they were quenched by addition of H_2SO_4 and hydroxylamine to final concentrations of 50 and 500 mM, respectively. The quenched solutions were subjected to centrifugation for 15 min at 14000*g* to pellet precipitated material, and 20 μL aliquots were injected onto a Zorbax SB-CN (4.6 mm × 250 mm, 5 μm) column (Agilent) that had been equilibrated in 95% solvent A (0.4% trifluoroacetic acid and 100 mM hydroxylamine, titrated to pH 1.78 with triethylamine) and 5% methanol. Simultaneous linear gradients from 5 to 13% methanol and from 0 to 21% acetonitrile were applied from 0 to 7 min and then held constant for 24 min before returning to the original conditions. Detection was monitored at 260 nm for the first 10.4 min of the run, and then at 220 nm until the end of the run. Under these conditions, peptides **2** and **3** eluted with retention times of 20.4 and 17.6 min, respectively.

RESULTS

Cloning and Expression of the K. pneumoniae atsB Gene and Purification of AtsB. The *atsB* gene of *K. pneumoniae* was cloned into the *Nde*I and *Eco*RI sites of expression vector pET-28a by standard methods. This construct allows production of the encoded protein with an N-terminal hexahistidine tag that is separated from the natural start codon by a spacer of 10 amino acids, facilitating rapid purification of the protein under anaerobic conditions. Subsequent sequencing of the gene revealed several changes in the DNA sequence that were not present in the published sequence of the *atsB* gene, and that resulted in amino acid changes. These amino acid changes include Gly140Ser, Val197Asp, Thr297Ala, Pro50Ser, and Ser284Leu. The first three amino acid changes have been observed previously and noted on the expasy proteomics server (http://ca.expasy.org/uniprot/Q9X758). The last two changes we confirmed by sequencing three independent clones from two independent cloning trials.

Because AtsB was predicted, and a homologue subsequently shown (*46*), to contain Fe/S clusters, the *atsB* gene was coexpressed with genes on plasmid pDB1282, which encodes an operon from *Azotobacter vinelandii* that is known to be involved in Fe/S cluster biosynthesis (*47, 48*). Plasmid pDB1282 confers resistance to ampicillin, while plasmid pAtsBWt, which is derived from commercially available pET-28a, confers resistance to kanamycin. The genes on plasmid pDB1282 were under the control of an arabinose-inducible promoter and were induced prior to the *atsB* gene, which was under the control of an IPTG-inducible promoter, to allow production of the proteins involved in Fe/S cluster biosynthesis before production of AtsB. Bacterial growth and protein overproduction were carried out in M9 minimal medium to obtain maximum incorporation of ^{57}Fe into the protein for analysis by Mössbauer spectroscopy.

AtsB was purified by cobalt IMAC inside an anaerobic chamber under an atmosphere of hydrogen (10%) and nitrogen (90%) gas. Initial attempts made use of Ni-NTA resin; however, the resulting protein was noticeably inhomogeneous (<90% pure) and contained two significant contaminants. Talon metal affinity resin (cobalt form) proved to be a fruitful alternative to Ni-NTA resin, which was used to purify hexahistidine-tagged AtsA. In Figure 1, an SDS−PAGE analysis of the purification of AtsB (lane 2) and AtsA (lane 3) is displayed. The amino acid sequences of hexahistidine-tagged AtsB and AtsA predict proteins with molecular masses of 46432 and 66319 Da, respectively, and are consistent with their migratory properties by SDS−PAGE.

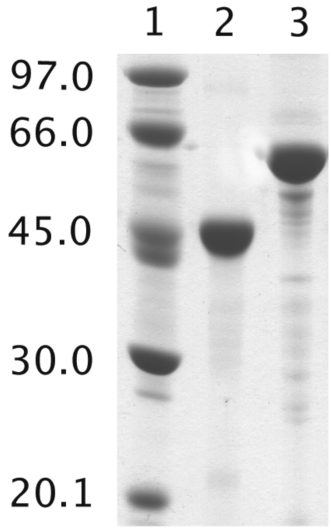

FIGURE 1: SDS−PAGE analysis of purified AtsB and AtsA (aa 21−578): lane 1, molecular mass markers; lane 2, AtsB (46431.9 Da) purified by IMAC using cobalt Talon affinity resin; and lane 3, AtsA (66318.9 Da) purified by IMAC using Ni-NTA resin. The gel was stained with Coomassie brilliant blue.

From 30 g of cell paste, ~30 mg of protein that is ≥95% pure is routinely isolated. The fairly low yield partly stems from the loss of protein during concentration steps; AtsB has a tendency to aggregate and form a membranous film on ultrafiltration filters. Inclusion of a peptide substrate during concentration greatly increases solubility and allows the protein to be concentrated to ≥500 μM. An AtsB triple variant, containing C → A substitutions at those cysteines within the RS signature CX_3CX_2C motif (Cys35, Cys39, and Cys42), was also constructed and purified as described for the WT protein.

Amino acid analysis was performed on AtsB to ascertain whether it is necessary to apply a correction factor to the Bradford protein determination assay. Two independent analyses were conducted at two different facilities. To minimize variability, it was necessary to ship defined quantities of lyophilized AtsB in appropriate vials, rather than in frozen solution, to which acid was added directly for hydrolysis. Results indicate that the Bradford assay, using BSA as a standard, underestimates the concentration of AtsB by a factor of 1.07 ± 0.05 (University of California, Davis, CA) or 1.05 ± 0.09 (Dana Farber Cancer Institute), indicating that, within experimental error, no correction is needed.

Spectroscopic Characterization of Wild-Type and C35A/C39A/C42A AtsB. The UV−vis spectrum of as-isolated (AI) AtsB is shown in Figure 2A (solid line) and is consistent with the presence of [4Fe-4S] clusters. The distinguishing features include the shoulder at 320 nm, the peak at 395 nm, and the broad tailing that extends beyond 700 nm. Iron and sulfide analyses of the AI protein indicate that each polypeptide contains 8.7 ± 0.4 iron atoms and 12.2 ± 2.6 sulfide atoms. To analyze the type and stoichiometry of Fe/S clusters more rigorously, Mössbauer spectroscopy was conducted on ^{57}Fe-enriched wild-type (WT) and C35A/C39A/C42A triple variant forms of AtsB. The spectrum of WT AtsB (Figure 3A) is dominated by an intense quadrupole doublet. Spectra collected over a wider range of Doppler velocities reveal that the sample contains only a small amount of one or more Fe species exhibiting a magnetically split

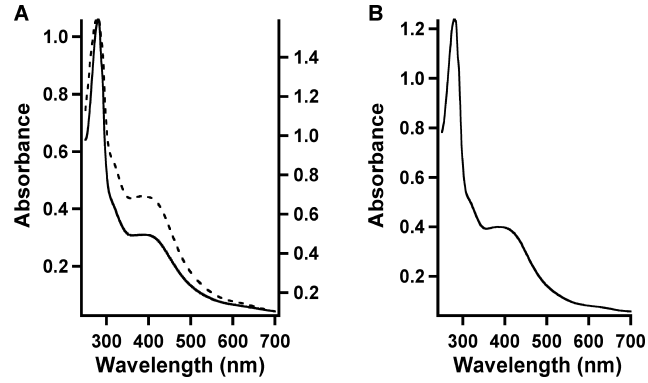

FIGURE 2: UV−visible spectra of (A) AI WT AtsB (9.88 μM, solid line, left *Y*-axis) and RCN WT AtsB (14.4 μM, dotted line, right *Y*-axis) and (B) AI C35A/C39A/C42A AtsB (11.9 μM). The A_{280}/A_{395} ratios of AI WT and RCN AtsB were 2.69 and 2.31, respectively. The A_{280}/A_{395} ratio of AI C35A/C39A/C42A AtsB was 3.12.

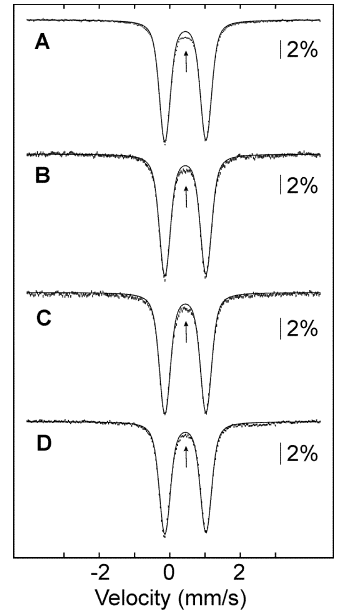

FIGURE 3: Mössbauer spectra of (A) AI WT AtsB, (B) RCN WT AtsB, (C) AI C35A/C39A/C42A AtsB, and (D) RCN C35A/C39A/C42A AtsB. All spectra were recorded at 4.2 K in an external 53 mT magnetic field. The solid lines in parts A−D represent a quadrupole doublet with the following parameters: $\delta = 0.44$ mm/s and $\Delta E_Q = 1.17$ mm/s.

subspectrum. The EPR spectrum of an identical sample reveals a small amount of a $[3Fe\text{-}4S]^+$ cluster (~10 μM), which corresponds to ~1% of the total Fe contained in the sample (3 × 10 μM/3.95 mM Fe). The Mössbauer spectra of a $[3Fe\text{-}4S]^+$ cluster are the superposition of three magnetically split subspectra, corresponding to the three distinct Fe sites (*49*). Since their features are relatively broad and similar for different $[3Fe\text{-}4S]^+$ clusters (*49*), the 1% contribution of the $[3Fe\text{-}4S]^+$ clusters is beyond the detection limit of Mössbauer spectroscopy. The spectrum can be analyzed assuming one broad quadrupole doublet with parameters typical of $[4Fe\text{-}4S]^{2+}$ clusters: isomer shift (δ) of 0.44 mm/s and quadrupole splitting parameter (ΔE_Q) of 1.17 mm/s. This quadrupole doublet accounts for 94 ± 3% of the total Fe (solid line in Figure 3A). The weak absorption at ~0.7 mm/s (see arrow) is consistent with the position of the high-energy line of the spectrum of $[2Fe\text{-}2S]^{2+}$ clusters. The sample, thus, may contain a small amount (<3%) of this cluster type. In

combination with the ratio of 8.7 iron atoms per AtsB polypeptide, these experiments indicate that AI WT AtsB contains 2.0 [4Fe-4S] clusters per polypeptide.

Upon reconstitution of the protein with additional ^{57}Fe and sulfide, followed by gel filtration on Sephadex G-25 resin, AtsB was found to contain 12.3 ± 0.2 irons and 9.9 ± 0.4 sulfides per polypeptide. The UV−vis spectrum of the reconstituted (RCN) protein (Figure 2A, dashed line) shows an increased absorption at 395 nm, and a lower A_{280}/A_{395} ratio as compared to that of the AI protein (2.31 and 2.69, respectively). The 4.2 K, 53 mT Mössbauer spectrum (Figure 3B) of reconstituted WT AtsB is identical within experimental uncertainty to that of AI WT AtsB. The solid line is a simulation using the same parameters (δ = 0.44 mm/s; ΔE_Q = 1.17 mm/s; 94% of total Fe). Therefore, virtually all of the iron present in the reconstituted sample is of the [4Fe-4S]$^{2+}$ configuration, indicating that RCN WT AtsB contains three [4Fe-4S] clusters per polypeptide.

The finding of three [4Fe-4S] clusters per polypeptide is corroborated by site-directed mutagenesis studies, wherein all Cys residues in the CX_3CX_2C motif are changed to Ala. The UV−vis spectrum of the AI triple variant (Figure 2B) is quite similar to that of WT AtsB; it maintains the shoulder at 320 nm, the peak at 395 nm, and the broad tailing that extends beyond 700 nm, suggesting that although all ligands to the RS cluster have been removed, [4Fe-4S] clusters are still associated with the protein. Analyses for iron and sulfide indicate the presence of 7.3 ± 0.1 irons and 7.2 ± 0.2 sulfides, consistent with the presence of two [4Fe-4S] clusters associated with this protein. The Mössbauer spectrum of the triple variant is dominated by a quadrupole doublet with parameters identical to those of WT AtsB [δ = 0.44 mm/s; ΔE_Q = 1.17 mm/s; 94% of intensity (Figure 3C)]. A stoichiometry of 1.7 [4Fe-4S] clusters per polypeptide is deduced from the relative intensity of the quadrupole doublet (94 ± 3% of the total Fe), and the Fe/AtsB ratio of 7.3, indicating the presence of two remaining [4Fe-4S] clusters in the AtsB triple variant. When the triple variant was subjected to reconstitution conditions, 7.7 ± 0.1 and 8.4 ± 0.4 sulfides per polypeptide were found to be associated with the protein, indicating that, unlike the WT protein, the triple variant was unable to incorporate a third Fe/S cluster. The Mössbauer spectrum of the RCN triple variant (Figure 3D) is essentially identical to that of the AI triple variant. It shows a quadrupole doublet with the same parameters as the AI triple variant, which accounts for 93% of the spectral intensity.

Time-Dependent Formation of Formylglycine and 5′-Deoxyadenosine. In Figure 4, MALDI mass spectra of the AtsB-catalyzed reaction are displayed. Each reaction was performed using 2 mM dithionite as the requisite reductant, and each mixture contained 1 mM peptide **1** and 100 μM AtsB. Spectrum A in Figure 4 is that of an assay mixture containing all components except AtsB (t = 0), which was then mixed with 100 mM phenylhydrazine before it was spotted onto a MALDI plate. The dominant feature in the spectrum has an m/z value of 1961.5, which corresponds to the molecular mass of the unmodified substrate. After addition of AtsB and a further incubation for 60 min, the magnitude of the peak at m/z 1961.5 decreases dramatically (almost completely), and a new peak having an m/z value of 2049.5 appears, which is consistent with the phenylhydrazine adduct of a FGly-containing product (spectrum B). Displayed in spectrum C is a reaction in which the Flv/Flx/NADPH reducing system is substituted for dithionite. Although a phenylhydrazine adduct of an FGly product is observed, the quantity of the product is substantially reduced compared to that observed in the presence of dithionite.

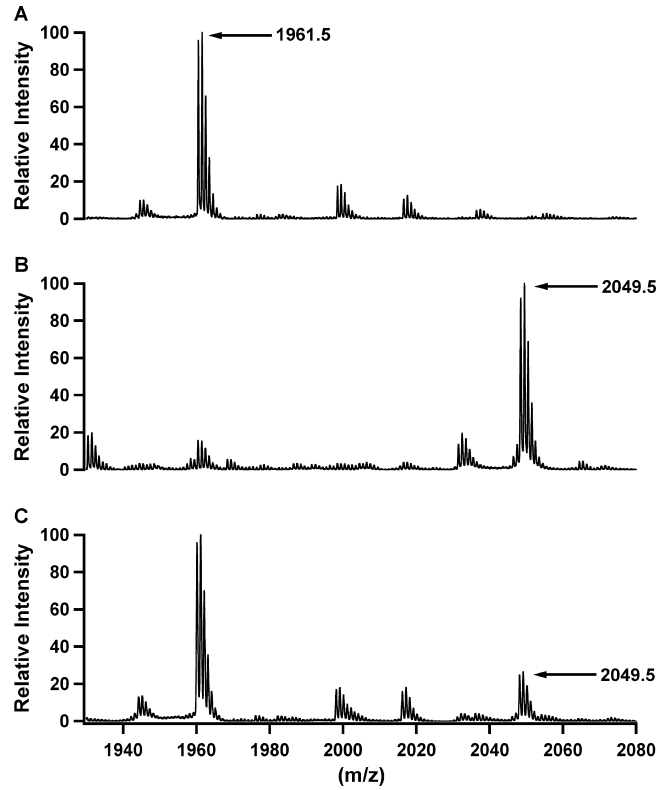

FIGURE 4: Demonstration of FGly formation by MALDI-MS in the presence of phenylhydrazine. The reaction mixture contained 100 μM AI WT AtsB, 1 mM SAM, 2 mM peptide **1** (m/z 1961.5), and 2 mM dithionite: (A) t = 0 and (B) t = 60 min. Reactions were quenched in 1 M HCl containing 100 mM phenylhydrazine, and mixtures were spotted on a MALDI target plate as described in Materials and Methods. The phenylhydrazine adduct displays a peak at m/z 2049.5. (C) t = 60 min for the reaction using the Flv/Flx/NADPH reducing system.

In the absence of phenylhydrazine, two product peaks are observed (Figure 5, solid line). One product peak corresponds to the expected value of m/z 1958.6, indicating the presence of the aldehyde, while a second, much larger, peak corresponds to an m/z value of 1940.6. The difference in m/z values between these two peaks is 18.0, suggesting that the equivalent of a molecule of water is eliminated from the FGly product. Consistent with this conclusion, the shift occurs only under turnover conditions using an appropriate substrate. In this particular experiment, the ratio of the magnitude of the peak at m/z 1958.6 to that at m/z 1940.6 is ~0.3; however, it was found to be variable from experiment to experiment and probably reflects subtle differences in preparing and spotting samples for analysis by MALDI-MS, since the ratios were consistent for samples spotted on the same plate. In fact, in some experiments, the overwhelming majority of product was found at m/z 1958.6. Since the N-termini of the peptide substrates used were not blocked, we suggest that the peak at m/z 1940.6 corresponds to formation of a Schiff base between the N-terminal amino group and the FGly residue. When a peptide substrate containing an acetylated

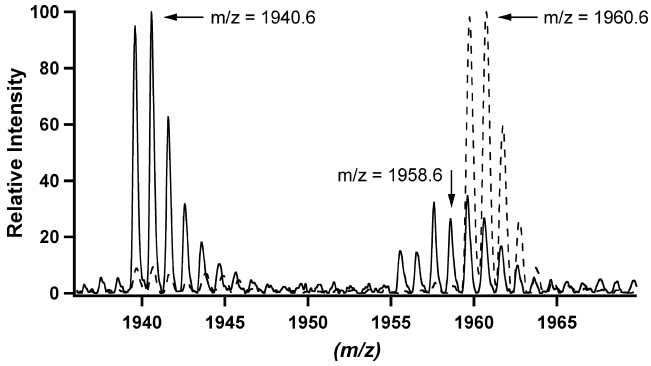

FIGURE 5: Quantification of FGly formation by MALDI-MS in the absence of phenylhydrazine. The reaction mixture contained 100 μM AI WT AtsB, 1 mM SAM, 2 mM peptide **1** (*m/z* 1960.6), and 2 mM dithionite. Reactions were quenched in 1 M HCl, and then mixtures were spotted on a MALDI target plate as described in Materials and Methods: $t = 0$ (---) and $t = 20$ min (—). The peak at *m/z* 1940.6 corresponds to the dehydration product from formation of a Schiff base between the FGly product (*m/z* 1958.6) and presumably the N-terminal amino group.

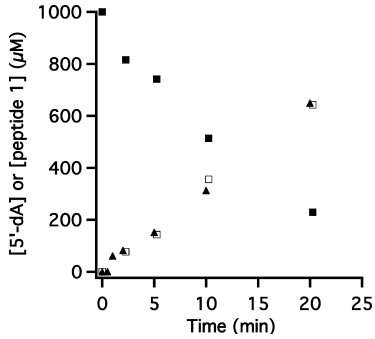

FIGURE 6: Stoichiometry of formation of 5′-dA and FGly. The reaction mixture contained 100 μM AI WT AtsB, 1 mM SAM, 1 mM peptide **1**, and 2 mM dithionite. FGly formation (□) and substrate peptide loss (■) were detected by MALDI-MS in the absence of phenylhydrazine and quantified from the intensities of the appropriate peaks according to the equation $[P] = \{(x + y)/[x + y + (z - 0.25y)]\}[S]$, where [P] and [S] correspond to FGly and substrate peptide concentrations, respectively, and x, y, and z correspond to the peak intensities at *m/z* 1940.6, 1958.6, and 1960.6, respectively. The appearance of 5′-dA (▲) was monitored by HPLC as previously described in Materials and Methods.

N-terminus was used (peptide **2**), the corresponding FGly-containing product, but not the substrate, was barely detectable (data not shown). This lack of detection was not due to poor turnover, since the phenylhydrazine derivative of the product was observed with ease, and the substrate peak became less intense as a function of the extent of turnover.

Time-dependent quantification of FGly and 5′-dA was performed to extract rate constants for the reaction and is shown in Figure 6. Formation of 5′-dA was quantified by methods previously established in our laboratory (*47*), while the ratio of the sum of the peaks at *m/z* 1940.6 (dehydrated product) and *m/z* 1958.6 (FGly product) to that at *m/z* 1960.6 (peptide substrate) was used to quantify FGly, with the assumption that both substrate and product peptides are desorbed to similar extents. A careful study of the characterization of FGly adducts in peptides by MALDI time-of-flight (TOF) MS has shown that this assumption is not valid when evaluating formation of the phenylhydrazine adduct of the FGly-containing product, since it is desorbed to a much greater extent than the substrate (*50*). However, since the substrate and product peptides differ by only the equivalent of a molecule of water, these two species should behave similarly during MALDI-MS. The equation $[P] = \{(x + y)/[x + y + (z - 0.25y)]\}[S]$ describes calculation of the FGly product concentration, [P], for each time point, where x, y, and z are the peak intensities at *m/z* 1940.6, 1958.6, and 1960.6, respectively, and [S] is the starting substrate concentration. The time-dependent formation of FGly (□) is approximately linear over the 20 min span of the assay, as is the loss of the peptide substrate (■). This observation of linearity, even when more than 60% of the substrate is consumed, suggests that the reaction is most likely irreversible, the K_m for the substrate is relatively low, and the products of the reaction do not inhibit it to a significant extent. Within the time frame of the assay, >600 μM product is formed in the presence of 100 μM enzyme, indicating that unlike the RS enzymes lipoyl synthase (*47, 51*), biotin synthase (*52–54*), and MiaB protein (*55*) AtsB catalyzes multiple turnovers. The extent of turnover may even be underestimated, since the fraction of enzyme in the active state was not determined. Values for $V_{max}/[E_T]$ of 0.32 ± 0.01 and 0.36 ± 0.03 min^{-1} for formation of FGly and loss of peptide **1**, respectively, were determined from linear fits of the corresponding data. The time-dependent quantification of 5′-dA from the same assay afforded a $V_{max}/[E_T]$ of 0.32 ± 0.01 min^{-1}, similar to that for production of FGly.

Stoichiometry of the AtsB Reaction. A second, HPLC-based, method was also developed for monitoring time-dependent formation of FGly and 5′-dA. Reactions were quenched in the presence of hydroxylamine, which was also included in the mobile phase during product analysis by HPLC, as it facilitated separation of the substrate peptide from the FGly-containing product peptide. HPLC traces of the AtsB reaction, quenched at 0 (solid black line), 5 (dotted line), 10 (dashed line), and 20 min (solid gray line), are displayed in Figure 7A. The intensity of the peak corresponding to the substrate (peptide **2**) decreases as a function of time, and three new peaks, labeled **1**, **2**, and **3**, appear at retention times of 10.6, 12.1, and 12.7 min, respectively. In addition, the peak corresponding to 5′-dA (retention time, 5.8 min) increases as a function of the extent of reaction. A control reaction is shown in Figure 7B, in which the AtsB C35A/C39A/C42A triple variant was substituted for the WT protein. The spectra at 0 and 20 min overlay almost perfectly, and no formation of 5′-dA is observed. The peak at a retention time of 12.1 min is present at time zero but only increases in magnitude in the presence of an active catalyst. When peptide **2** was replaced with peptide **4**, which contains an Ala substitution at the target Ser residue, no production of peptide-related product peaks was observed. Figure 8A shows the time-dependent formation of FGly and 5′-dA (□ and ▲, respectively; left *Y*-axis), and the concomitant time-dependent loss of substrate, peptide **2** (■; right *Y*-axis), using dithionite as the requisite reductant. The concentration of the FGly product or remaining substrate was calculated from the ratio of the corrected areas (tryptophan standard) of the product peaks (sum of peaks 1, 2, and 3) to the area of the substrate peak, multiplied by 1000 μM, the initial substrate concentration. The concentrations of 5′-dA and the peptide product at each time point are similar in magnitude, as are the rate constants ($V_{max}/[E_T]$) for formation of each, 0.38 ± 0.01 and 0.36 ± 0.01 min^{-1}, respectively. Moreover,

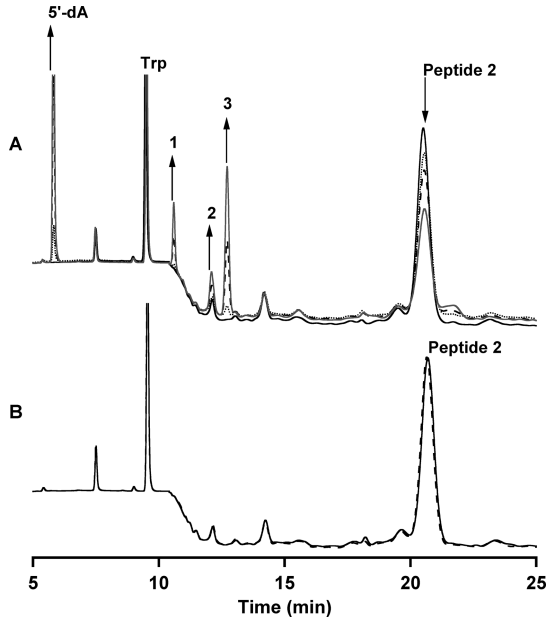

FIGURE 7: HPLC detection of formylglycine formation. Reaction mixtures contained 50 μM AtsB WT or C35A/C39A/C42A triple variant, 1 mM SAM, 2 mM dithionite, 1 mM tryptophan (IS), and 1 mM peptide **2**, and reactions were quenched in 100 mM H_2SO_4 containing 1 M hydroxylamine. (A) HPLC trace of the reaction in the presence of AI WT AtsB: 0 (solid black line), 5 (dotted line), 10 (dashed line), and 20 min (solid gray line). Directional arrows correspond to increases or decreases in peaks that undergo turnover-dependent changes. Retention times were as follows: 5.8 min for 5′-dA, 9.8 min for L-tryptophan, 10.6 min for peak 1, 12.1 min for peak 2, 12.7 min for peak 3, and 20.4 min for peptide **2**. (B) HPLC trace of the reaction in the presence of the AtsB C35A/C39A/C42A triple variant: 0 (solid black line) and 20 min (dashed line). The sloping baseline observed from 10.4 to 12 min results from decreasing concentrations of TFA in the applied gradient. This is noticeable because of a change in the detection wavelength at 10.4 min from 260 to 220 nm, wherein absorption by TFA becomes significant.

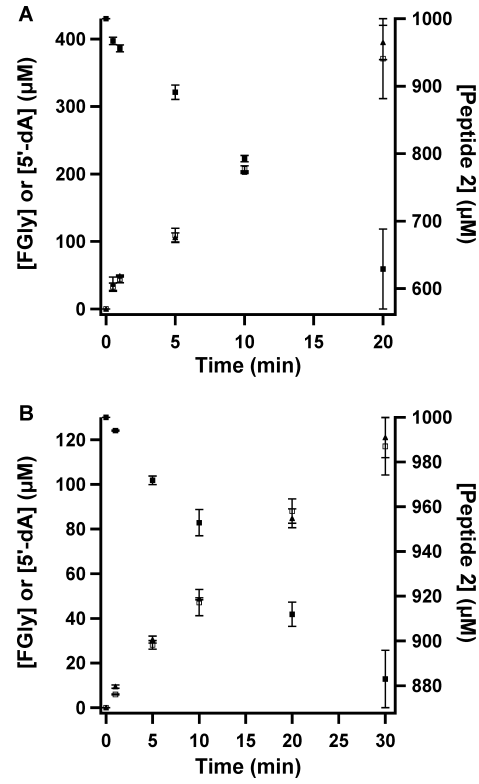

FIGURE 8: Time-dependent formation of 5′-dA (▲; left *Y*-axis) and FGly (□; left *Y*-axis) and depletion of peptide **2** (■; right *Y*-axis). Reaction mixtures contained 50 μM AtsB, 1 mM SAM, 1 mM peptide **2**, 2 mM tryptophan (IS), and dithionite (A) or 100 μM AtsB, 25 μM Flv, 5 μM Flx, and 2 mM NADPH (B). The data are the averages of two independent trials, and error bars denote one standard deviation.

the rate constants agree well with those obtained using MADLI-MS to quantify FGly formation. After reaction for 20 min, more than six turnovers per AtsB are observed. The results of FGly quantification by HPLC are consistent with those from quantification by MALDI-MS and indicate that the generation of one FGly modification requires the expenditure of 1 equiv of SAM.

Since dithionite is not a physiologically relevant reductant, experiments were performed to ascertain whether *E. coli* flavodoxin could support turnover. Flavodoxin is a flavin mononucleotide-containing protein that supplies reducing equivalents to a number of proteins (*56*), including RS proteins (*47, 57–59*) and methionine synthase (*60*). The proteins from *E. coli* and *K. pneumoniae* are 96% identical, suggesting that the *E. coli* enzyme should be a suitable substitute. When the Flv/Flx/NADPH reducing system is used to supply the requisite electron, the rate of product formation diminishes dramatically, exhibiting $V_{max}/[E_T]$ values of 0.039 ± 0.002 for formation of both 5′-dA [Figure 8B (▲)] and the FGly-containing peptide [Figure 8B (□)].

AtsB Can Act as a Cys-Type FGE. As discussed in the introductory section, AtsB from *K. pneumoniae* is a Ser-type anaerobic FGE, as its normal substrate contains a conserved seryl residue that is converted to FGly. However, anaerobic FGEs from *P. aeruginosa* and *Clostridium perfringens* are Cys-type enzymes (*2, 16*). In vivo studies in *E. coli* indicate that the sulfatase from *P. aeruginosa* can be activated by endogenous FGEs (*17*), whereas activation of AtsA from *K. pneumoniae*, a Ser-type sulfatase, requires cotransformation of the *atsA* and *atsB* genes (*21*). Given that the FGE from *C. perfringens* is also a RS protein (*46*), the mechanism of FGly generation in anaerobic Ser-type and Cys-type FGEs is likely to be similar. Figure 9 shows turnover by AtsB in the presence of peptide **3**, which contains a Cys substitution at the target Ser. Using dithionite as the reductant, AtsB catalyzed formation of the FGly modification with a $V_{max}/[E_T]$ of 1.14 ± 0.12 min^{-1} [Figure 9A (□)], which is more than 3-fold greater than that observed using peptide **2** (0.32 ± 0.01 min^{-1}). There also appears to be some uncoupling of SAM cleavage with respect to FGly generation; the $V_{max}/[E_T]$ for 5′-dA is 1.59 ± 0.21 min^{-1} [Figure 9A (▲)], and the ratio of 5′-dA to FGly grows larger as a function of time. In the presence of the Flv/Flx/NADPH reducing system, the $V_{max}/[E_T]$ for formation of both 5′-dA [Figure 9B (▲)] and the FGly modification [Figure 9B (□)] is 0.018 ± 0.001 min^{-1}.

DISCUSSION

Purification and Characterization of AtsB. The AtsB-catalyzed oxidation of an alcohol to an aldehyde is an intriguing reaction, because it avoids use of cofactors that are typically employed in these types of transformations, such as those that contain pyridine or flavin nucleotides. Given our interest in characterizing RS enzymes that contain multiple Fe/S clusters (*42, 51*), and the prediction by

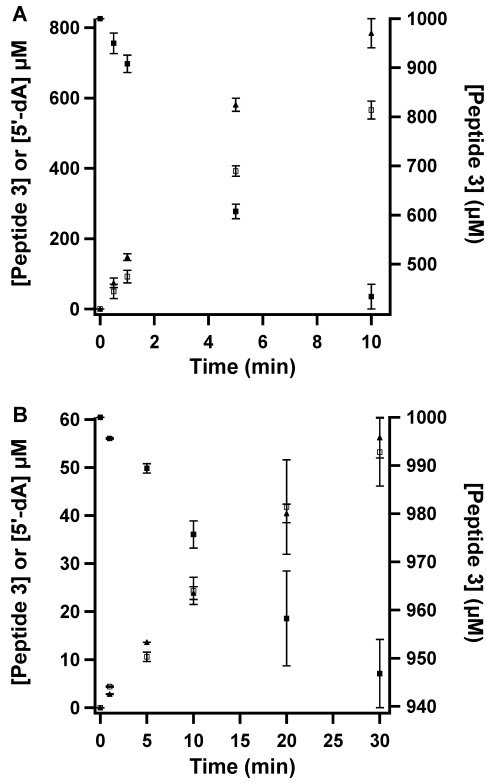

FIGURE 9: Time-dependent formation of 5′-dA (▲; left *Y*-axis) and FGly (□; left *Y*-axis) and depletion of peptide **3** (■; right *Y*-axis). Reaction mixtures contained 50 μM AtsB, 1 mM SAM, 1 mM peptide **3**, 2 mM 1 mM tryptophan (IS), and dithionite (A) or 100 μM AtsB, 25 μM Flv, 5 μM Flx, and 2 mM NADPH (B). The data are the averages of two independent trials, and error bars denote one standard deviation.

bioinformatics methods that AtsB contains three (*2*), we sought to clone the *atsB* gene from *K. pneumoniae* and characterize its protein product and reaction. Although catalytically active AtsB has been difficult to purify, as evidenced by its intense study only in cell lysates (*22, 23*), we employed a previously developed strategy, in which the *atsB* gene was coexpressed with genes from an *A. vinelandii* operon that are known to be involved in Fe/S cluster biosynthesis (*47, 48, 61*). This strategy allowed the hexahistidine-tagged protein to be purified under anaerobic conditions, affording 5 mg of product per liter of growth medium. The inclusion of a peptide substrate during cell lysis as well as steps that involve concentration by ultrafiltration greatly enhanced the protein's stability, solubility, and final yield. Analysis of iron and sulfide on a preparation of AI, ^{57}Fe-labeled protein indicated that it contained 8.7 ± 0.4 irons and 12.2 ± 2.6 sulfides per polypeptide; however, these stoichiometries varied from ~8 to 12 irons and sulfides among different preparations. Characterization of the ^{57}Fe-labeled protein after reconstitution with additional ^{57}Fe and sulfide provided strong evidence for the presence of three [4Fe-4S] clusters; the protein contained 12.3 ± 0.2 irons and 9.9 ± 0.4 sulfides per polypeptide, of which 94% of the iron was shown by Mössbauer spectroscopy to exist in the form of cubane $[4Fe\text{-}4S]^{2+}$ clusters (2.9 clusters per polypeptide). The finding that 7.3 ± 0.1 irons and 7.2 ± 0.2 sulfides remained with the C35A/C39A/C42A triple variant, and that 94% of all of the iron was in the form of $[4Fe\text{-}4S]^{2+}$ clusters (1.7 clusters per polypeptide), clearly supports the argument for three [4Fe-4S] clusters per polypeptide. This argument is further strengthened by the finding that the iron and sulfur content does not change significantly upon reconstitution of the triple variant.

Stoichiometry of the AtsB Reaction. The oxidation of a seryl residue to FGly results in a mass change of −2 and also affords a functional group not typically observed in proteins. In previous studies, MALDI-MS was often used to qualitatively assess turnover, exploiting the reactivity of the functional group with phenylhydrazine or 2,4-dinitrophenylhydrazine (*16, 22, 23, 46, 50*). The adduct formed allows clear separation of the substrate and product peaks; however, the ratio of product to remaining substrate cannot be used to quantify the extent of turnover, because the adduct-containing product is desorbed significantly better than the unmodified substrate (*50*). We, therefore, quantified product formation in the absence of derivatization using an 18 aa peptide substrate taken from a region of AtsA from *K. pneumoniae* that contained the target seryl residue and other highly conserved aa residues. When a substrate containing a free amine at the N-terminus was employed, two product peaks were observed by MALDI-MS. One corresponded to the peptide containing an FGly modification generated from a seryl residue, while the other appeared to be a dehydration product of the FGly-modified peptide, wherein Schiff base formation occurred between the free amine and the aldehyde. Acetylation of the N-terminal amine suppressed formation of the putative cyclized product but also negatively affected the ability of the peptide to be monitored by MALDI-MS, especially the product peptide containing the FGly modification. Rate constants, however, could be determined for the reaction that included the unblocked peptide substrate by accounting for the two products formed. Quantification of FGly formation by MALDI-MS was performed using only dithionite as the reductant; however, it is worthwhile to note that formation of 5′-dA and the FGly peptide occurred with the same rate constants (0.32 ± 0.01 and 0.32 ± 0.01 min^{-1}, respectively), indicating that the AtsB-catalyzed oxidation of a seryl residue to a FGly residue requires the expenditure of one molecule of SAM.

A second, HPLC-based assay was also developed to quantify turnover and verify the conclusions reached using the MS-based assay. This method also had associated caveats, the most significant being that during analysis by HPLC three product peaks were formed. Although we have yet to characterize these peaks definitively, they appear only under turnover conditions and are associated with the peptide substrate and not SAM cleavage products. Our best guess at this time is that they represent different adducts of the FGly modification. Nevertheless, each of these peaks reproducibly behaved similarly as a function of time, and the ratio of the sum of their areas to that of the peptide substrate afforded rate constants (0.36 ± 0.01 min^{-1}) that were similar to those obtained by MALDI-MS (0.32 ± 0.01 min^{-1}). Again, this rate constant agrees well with that obtained for formation of 5′-dA (0.38 ± 0.01 min^{-1}). Moreover, the same 1:1 stoichiometry was also observed in the presence of the physiological reducing system (Flv/Flx/NADPH), although the rate constants were considerably smaller (0.039 ± 0.002 min^{-1} for formation of both 5′-dA and FGly).

The slower turnover observed in the presence of the Flv/Flx/NADPH reducing system is not unexpected, since the

redox potentials of Fe/S clusters in RS enzymes tend to be on par with, or higher than, that of dithionite, but significantly lower than that of flavodoxin (*57, 62, 63*). The slower turnover rate is observed because the equilibrium concentration of enzyme poised to initiate cleavage of SAM in the presence of reduced flavodoxin is considerably lower than that in the presence of dithionite. In fact, the presence of reduced flavodoxin typically does not allow EPR-detectable reduction of the Fe/S cluster(s) of RS enzymes. Nevertheless, the $V_{max}/[E_T]$ for AtsB using flavodoxin as reductant is not dissimilar to single-turnover rate constants reported for biotin synthase (0.07 min^{-1}) (*54*) and lipoyl synthase (0.175 min^{-1}) (*47*) obtained under similar conditions.

One issue not addressed in this study pertains to the stoichiometry of reducing equivalents in the reaction. The AtsB reaction is a two-electron oxidation of an alcohol to an aldehyde. One oxidizing equivalent is provided by the 5′-dA• generated from the cleavage of SAM. This cleavage reaction occurs in a reductive fashion, requiring the input of one electron. The nature of the ultimate acceptor of the second electron is not readily apparent, although the electron might reside transiently on one of the three Fe/S clusters. One possibility is that the second electron is used as the required reducing equivalent for subsequent rounds of SAM cleavage during catalytic turnover. If this were the case, however, it might be expected that in reactions in which the Flv/Flx/NADPH reducing system is employed, a lag, corresponding to slow initial reduction of the RS [4Fe-4S] cluster by reduced Flv, would be followed by a faster phase, corresponding to internal reduction of the RS cluster as a result of turnover. This is not observed, however, in these preliminary studies. In the presence of the Flv/Flx/NADPH reducing system, there appears to be no lag; the rate of product formation is linear throughout the course of the activity determination. AtsB may operate like the RS protein HemN, wherein an unidentified protein or small molecule is proposed to serve as an electron acceptor (*64*). Alternative electron acceptors, such as oxidized DTT, might serve this function in our assays.

Possible Roles for Additional Clusters in the AtsB Reaction. K. pneumoniae AtsB contains 13 cysteinyl residues, 12 of which have been characterized as residing in three conserved motifs (*2*). Motif I consists of the cysteines within the $C^{35}X_3C^{39}X_2C^{42}$ RS sequence and is found near the N-terminus of the protein. Another cysteine, originally considered to reside in motif I, is found 85 aa C-terminal to Cys42. The eight remaining cysteines are found in the C-terminal region of the protein, residing in motifs II ($C^{270}X_5C^{276}X_{14}C^{291}$) and III ($C^{331}X_2C^{334}X_5C^{340}X_3C^{344}$-$X_{12}C^{357}$). We envision that some of these cysteinyl residues contribute ligands to the two additional [4Fe-4S] clusters observed in this study; however, with the exception of the RS cysteine sequence, we do not know whether cysteines in any given motif all contribute ligands to the same cluster. For example, one cluster might contain two cysteinyl ligands from motif II and two cysteinyl ligands from motif III, while another cluster might contain one cysteinyl ligand from motif II and two or three from motif III. Several cysteinyl residues within the three motifs have been changed to alanyl residues to assess their importance in catalysis by AtsB. Variant proteins containing Cys → Ala substitutions at Cys39, Cys42, Cys270, Cys331, and Cys334 were unable to activate AtsA when their genes were coexpressed in *E. coli* with the *atsA* gene. Biochemical characterization of AtsA isolated from cotransformed cells indicated no evidence of the FGly cofactor (*23*).

Our original interest in AtsB stemmed from the possibility that the protein might use a second Fe/S cluster in a sacrificial manner, as proposed for LS, BS, and MiaB protein (*51*). In this scenario, abstraction of a hydrogen atom from C-3 of the target seryl residue would be followed by sulfur insertion from the second Fe/S cluster to yield a geminal hydroxy thiol intermediate, which would collapse to the aldehyde with concomitant elimination of sulfide. This mechanism predicts that AtsB should catalyze only one turnover, since it would act as both a catalyst and a substrate (*51*). Results presented in this study show, however, that in the presence of dithionite, approximately eight turnovers are observed during a 20 min incubation, and indeed, 50 μM AtsB is capable of converting 1 mM substrate to product within 60 min of incubation at 37 °C. Therefore, a mechanism involving cryptic sulfur insertion is ruled out.

A working hypothesis for the mechanism of the AtsB reaction that is consistent with the results of this study is shown in Scheme 2. In this mechanism, one of the remaining two Fe/S clusters is ligated by only three cysteines, providing an open coordination site to which the hydroxyl group of the target seryl residue can bind, which is found in aconitase (*65*) and proposed in serine dehydratase (*66*) and other Fe/S cluster-dependent enzymes within the hydrolyase family (*67*). This coordination would facilitate two processes: it would decrease the pK_a for deprotonation of the alcohol prior to or subsequent to abstraction of a hydrogen atom from C-3 of the target seryl residue by 5′-dA• (*68*), and it would allow for facile inner-sphere electron transfer to the cluster (*68*). The mechanism in Scheme 2 shows deprotonation of the coordinated hydroxyl group as the first step in the reaction, because it would facilitate subsequent abstraction of a hydrogen atom from C-3 of the target Ser residue as a result of resonance delocalization (step 3). Gas-phase homolytic bond dissociation energies (BDEs) have been measured and/or calculated for carbon-centered methanol and methoxide radicals. The observed BDE for generating the former is 91.8 ± 1.2 kcal/mol (*69, 70*) and is calculated to decrease by 16.5 kcal/mol in generation of the latter (*70*). In addition, ligation of the hydroxyl group to an iron atom of the Fe/S cluster is also likely to lower the BDE significantly. Abstraction of a C-3 hydrogen atom from the target seryl residue by 5′-dA• is then followed by an inner-sphere electron transfer to generate the aldehyde product, with concomitant one-electron reduction of the coordinating cluster (step 4). The last step would be transfer of one electron to an appropriate acceptor (step 5), which in vivo may be flavodoxin, itself. The results presented herein do not support a mechanism in which the electron is returned to the RS Fe/S cluster to allow for subsequent SAM cleavage in the absence of external reductant, although more detailed studies are needed to address this issue unambiguously.

The first example of in vitro turnover of an anaerobic FGE has already been reported, in which a "Cys-type" FGE from *C. perfringens* was produced recombinantly in *E. coli* and characterized (*46*). As expected from its sequence homology to *K. pneumoniae* AtsB, which had been shown to be a member of the RS family of proteins, the protein contained

Scheme 2: Working Hypothesis for AtsB-Catalyzed FGly Formation (bold numbers represent individual steps)[a]

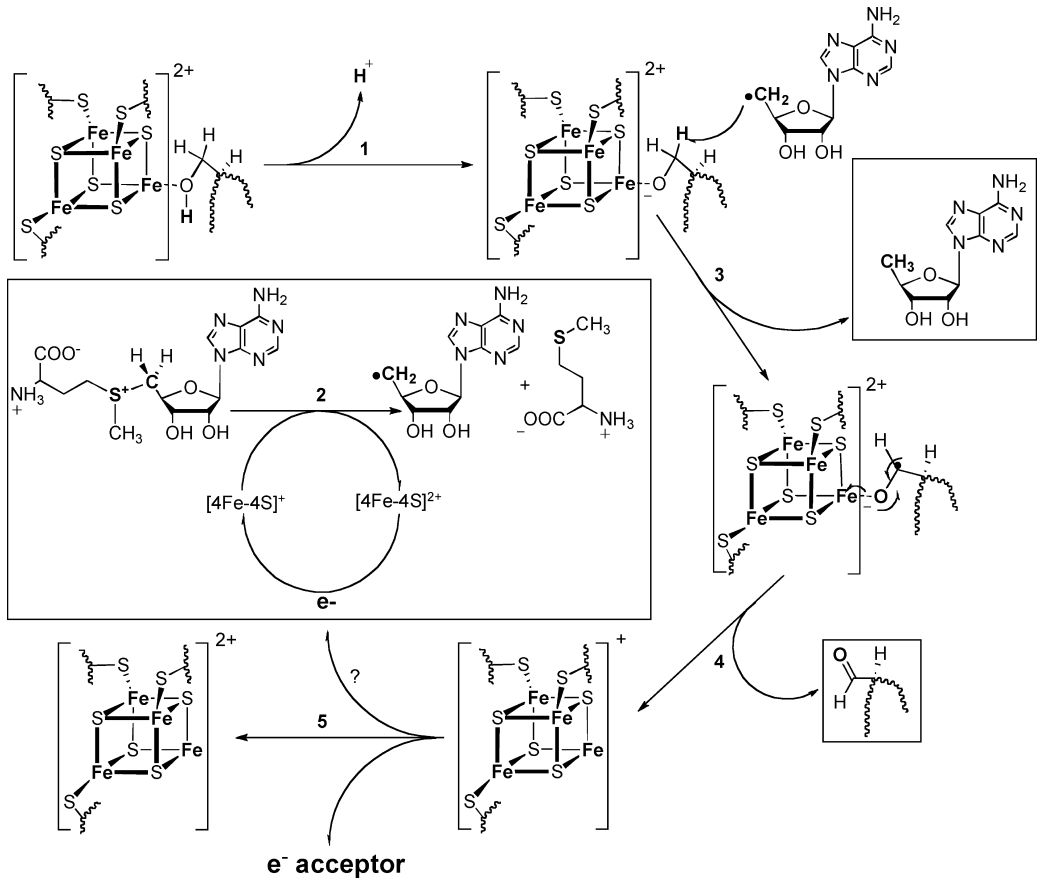

[a] The reaction is initiated by coordination of the hydroxyl group of the target seryl residue to an empty coordination site on one of the three Fe/S clusters. Subsequent to deprotonation (step 1) and generation of 5′-dA• (step 2), 5′-dA• abstracts a hydrogen atom from C-3 of the target seryl residue (step 3), which is followed by inner-sphere electron transfer and radical recombination to afford the FGly product and a one-electron reduced Fe/S cluster (step 4). Finally, the electron is transferred to an unidentified acceptor (step 5).

3.0 ± 0.2 mol of iron per mole of monomer in its AI form and exhibited a UV−vis spectrum that was consistent with the presence of Fe/S clusters. Upon reconstitution of the AI protein with a 10-fold excess of iron and sulfide followed by size exclusion chromatography to remove excess small molecules, the protein was found to contain 6.0 ± 0.3 mol of iron per monomer. Whether this excess iron was in the form of a [4Fe-4S] cluster was not rigorously determined; however, the magnitude of the absorption band at 420 nm in the UV−visible spectrum of the protein was observed to increase. We (*42*), and others (*71*), have found that proteins with adventitiously bound iron that arises from their reconstitution with iron and sulfide often display UV−vis spectra that are consistent with the presence of [4Fe-4S] clusters. Although this protein, when reconstituted, was capable of catalyzing formation of FGly at the target cysteinyl residue in a 23 aa peptide substrate, rates of turnover were not reported (*46*). The significant presence of starting material subsequent to long incubation times under turnover conditions (6 h with 40 μM protein) would suggest that this protein is intrinsically less active than AtsB, or that the preparation contains an abundance of inactive protein.

AtsB Can Act as a Cys-Type Anaerobic FGE. It has been suggested that the pathways for generating FGly from seryl versus cysteinyl residues by anaerobic FGEs are different (*22*). This conclusion is derived from two significant observations from in vivo activation studies of the Cys-type FGE from *P. aeruginosa* and AtsB from *K. pneumoniae*, a Ser-type FGE. Expression of the *P. aeruginosa atsA* gene in an arylsulfatase-deficient strain of *P. aeruginosa* restored the ability of the organism to grow on aromatic sulfate esters as its source of sulfur. When the strain was transformed with a plasmid encoding a Cys → Ser substitution at the target cysteinyl residue, growth on aromatic sulfate esters was abolished (*17*). Similar results were obtained when the *P. aeruginosa atsA* gene was transformed in *E. coli*. Isolation and characterization of the heterologously produced AtsA showed it to contain the FGly cofactor and to be catalytically active, suggesting that *E. coli* contains Cys-type FGEs (*17*). By contrast, AtsA from *K. pneumoniae* is not activated upon simple expression of its *atsA* gene; activation requires simultaneous expression of the *K. pneumoniae atsB* gene, suggesting that *E. coli* does not harbor a Ser-type FGE (*21*).

It is now clear that both Cys-type and Ser-type anaerobic FGEs are RS enzymes and that they presumably catalyze their respective reactions by very similar mechanisms (*23, 46*). In this study, we show that AtsB can indeed activate peptide substrates containing a Cys → Ser substitution at the seryl residue that is oxidized to FGly. In fact, the Cys-containing peptide affords a $V_{max}/[E_T]$ that is approximately 4-fold greater, suggesting that Cys-type sulfatases may be easier to activate by a radical mechanism than Ser-type sulfatases. The mechanism in Scheme 2 is consistent with our finding that AtsB can activate peptides containing Ser → Cys

substitutions at the position of relevance, as well as the observation that Cys-type anaerobic FGEs cannot activate Ser-type sulfatases or activate them very poorly. In step 1, the pK_a of a metal-bound cysteinyl residue would be expected to be significantly lower than that of a metal-bound seryl residue. The general base that removes that proton in a Cys-type anaerobic FGE might not be sufficiently strong to remove the proton from a metal-coordinated alcohol. In addition, abstraction of a hydrogen atom from C-3 of the substrate residue would be easier for the cysteinyl-containing substrate than the seryl-containing substrate, since the homolytic BDE for generating a carbon-centered methanethiol radical is on the order of 92 kcal/mol while the value for generating a carbon-centered methanol radical is on the order of 95 kcal/mol (*72*). The greater polarizability of the thiolate anion as compared to that of the alkoxide anion, both of which would be generated upon deprotonation of the respective metal-coordinated heteroatom, should allow for an increased level of stabilization of the carbon-centered methanethiolate radical as compared to the carbon-centered methoxide radical (*70*).

Very recently, subsequent to submission of this paper, another group produced complementary data that suggest that Cys-type and Ser-type anFGEs function by similar mechanisms (*73*). In this study, the authors cloned a gene from *Bacteroides thetaiotaomicron* that encodes a Ser-type RS anFGE and showed that the reconstituted protein was able to catalyze formation of 5′-dA in the presence of 23-mer peptides containing either Cys or Ser at the position of modification, with the cysteinyl-containing peptide supporting the greater amount of SAM cleavage. Interestingly, the level of 5′-dA formation was greatest in the absence of a peptide substrate; however, a peptide substrate containing an alanyl residue at the position of modification almost completely suppressed it. Similar behavior was observed with the Cys-type anFGE from *C. perfringens*, except that the level of 5′-dA formation in the absence of peptide was considerably lower. Additional in vitro and in vivo assays for qualitatively assessing FGly formation showed that both anFGEs were able to activate Ser-type and Cys-type sulfatases; however, the absence of kinetic resolution did not allow an accurate quantification of the efficiency (*73*).

Relationship of AtsB to Other RS Proteins. Enzymes within the RS superfamily catalyze a diverse array of reactions, including key steps in the biosynthesis of cofactors, coenzymes, antimicrobial agents, and herbicides, the biosynthesis and repair of DNA, the regulation of cellular function, and general metabolism (*25*). All of these reactions involve the common intermediate, 5′-deoxyadenosyl 5′-yl (5′-dA•), generated from a reductive cleavage of SAM (*28, 29, 74–76*). In an early review article on this superfamily, these enzymes were grouped into three classes, which were based on the net stoichiometry of 5′-dA and product generated (*77*). Class I enzymes were those that catalyzed the reversible cleavage of SAM, wherein a product radical abstracts a hydrogen atom from 5′-dA, initiating re-formation of SAM presumably via attack of 5′-dA• on L-methionine with concomitant transfer of an electron back to the cluster. Characterized members of class I enzymes include lysine 2,3-aminomutase (*27, 75*), a SAM-dependent glutamate mutase (*78*), and spore photoproduct lyase (*79–82*), which catalyzes the repair of the unique thymine dimer photoproduct, 5-thyminyl-5,6-dihydrothymine, found in UV-irradiated DNA of spores from *Bacillus subtilis*. Class II enzymes were those that catalyzed an irreversible cleavage of SAM but used 5′-dA• to generate a glycyl radical cofactor via abstraction of a hydrogen atom from the α-carbon of a specific glycine residue on a cognate protein (*83*). Glycyl radical cofactors initiate turnover by abstracting an appropriate hydrogen atom from a small-molecule substrate or a protein cysteinyl residue and are regenerated after each catalytic event. Therefore, the expenditure of one SAM molecule allows for multiple turnovers via creation of a radical-based cofactor. Several class II RS enzymes have been studied in vitro at varying levels of detail. The best characterized are the activating enzymes of the anaerobic ribonucleotide reductase and pyruvate formate-lyase, both from *E. coli* (*28, 29, 76, 84*).

At the time of the early review, very little was known about class III enzymes. These enzymes cleave SAM irreversibly for each hydrogen atom abstracted by 5′-dA• in a given reaction sequence. At this writing, six members have been characterized in moderate detail: biotin synthase (BS) (*85*), lipoyl synthase (LS) (*42, 86*), MiaB protein (*55, 87*), MoaA protein (*32*), coproporphyrinogen III oxidase (HemN) (*31*), and BtrN (*88*). The first three proteins catalyze insertion of sulfur into unactivated C−H bonds, representing the final step in the biosynthesis of biotin, lipoic acid cofactor, and the hypermodified tRNA nucleoside 2-methylthio-N^6-(isopentenyl)adenosine, respectively (*51*). In these reactions, evidence suggests that the inserted sulfur atom is derived from a second Fe/S cluster on the enzyme itself, and 1 equiv of SAM is cleaved irreversibly to 5′-dA for each sulfur−carbon bond that is formed (*51*). The last three enzymes catalyze key steps in the biosynthesis of molybdopterin, the anoxic biosynthesis of heme, and the biosynthesis of butirosin, a 2-deoxystreptamine-containing aminoglycoside antibiotic (*88*). BtrN catalyzes a reaction that is analogous to that of AtsB, which is the two-electron oxidation of a hydroxyl group to a ketone in the conversion of 3-amino-2,3-dideoxy-scyllo-inosamine to 3-amino-2,3-dideoxy-scyllo-inosose. Recent mechanistic analysis of this enzyme indicates a 1:1 stoichiometry of 5′-dA and product formation, which is observed for the AtsB reaction. However, the authors suggest that the extra electron is returned to the RS [4Fe-4S] cluster for subsequent rounds of SAM cleavage. At present, there is no experimental evidence that indicates that BtrN contains more than one [4Fe-4S] cluster per polypeptide; however, the primary structure of the protein contains eight cysteinyl residues. The studies presented herein indicate that AtsB also is a class III RS enzyme. Although it catalyzes multiple turnovers, it cleaves *S*-adenosyl-L-methionine irreversibly and stoichiometrically with respect to product formed. As is the case with HemN, which uses 5′-dA• to initiate a two-electron oxidative decarboxylation of coproporphyrinogen III (*31*), further studies are required to identify the acceptor of the second electron.

ACKNOWLEDGMENT

We thank Heike Betz at the Proteomics and Mass Spectrometry Core Facility for her assistance with MALDI-MS.

REFERENCES

1. Parenti, G., Meroni, G., and Ballabio, A. (1997) The sulfatase gene family. *Curr. Opin. Genet. Dev. 7*, 386–391.

2. Schirmer, A., and Kolter, R. (1998) Computational analysis of bacterial sulfatases and their modifying enzymes. *Chem. Biol. 5*, R181–R186.
3. von Figura, K., Schmidt, B., Selmer, T., and Dierks, T. (1998) A novel protein modification generating an aldehyde group in sulfatases: Its role in catalysis and disease. *BioEssays 20*, 505–510.
4. Hanson, S. R., Best, M. D., and Wong, C.-H. (2004) Sulfatases: Structure, mechanism biological activity, inhibition, and synthetic utility. *Angew. Chem., Int. Ed. 43*, 5736–5763.
5. Gadler, P., and Faber, K. (2007) New enzymes for biotransformations: Microbial alkyl sulfatases displaying stereo- and enantioselectivity. *Trends Biotechnol. 25*, 83–88.
6. Schmidt, B., Selmer, T., Ingendoh, A., and von Figura, K. (1995) A novel amino acid modification in sulfatases that is defective in multiple sulfatase deficiency. *Cell 82*, 271–278.
7. Müller, I., Kahnert, A., Pape, T., Sheldrick, G. M., Meyer-Klaucke, W., Dierks, T., Kertesz, M., and Usón, I. (2004) Crystal structure of the alkylsulfatase AtsK: Insights into the catalytic mechanism of the Fe(II) α-ketoglutarate-dependent dioxygenase superfamily. *Biochemistry 43*, 3075–3088.
8. Hagelueken, G., Adams, T. M., Wiehlmann, L., Widow, U., Kolmar, H., Tümmler, B., Heinz, D. W., and Chubert, W.-D. (2006) The crystal structure of SdsA1, an alkylsulfatase from *Pseudomonas aeruginosa*, defines a third class of sultatases. *Proc. Natl. Acad. Sci. U.S.A. 103*, 7631–7636.
9. Boltes, I., Czapinska, H., Kahnert, A., von Bülow, R., Dierks, T., Schmidt, B., von Figura, K., Kertesz, M. A., and Usón, I. (2001) 1.3 Å structure of arylsulfatase from *Pseudomonas aeruginosa* establishes the catalytic mechanism of sulfate ester cleavage in the sulfatase family. *Structure 9*, 483–491.
10. Dierks, T., Dickmanns, A., Preusser-Kunze, A., Schmidt, B., Mariappan, M., von Figura, K., Ficner, R., and Rudolph, M. G. (2005) Molecular basis for multiple sulfatase deficiency and mechanism for formylglycine generation of the human formylglycine-generating enzyme. *Cell 121*, 541–552.
11. Ghosh, D. (2007) Human sulfatases: A structural perspective to catalysis. *Cell. Mol. Life Sci. 64*, 2013–2022.
12. Dodgson, K. S., White, G. F., and Fitzgerald, J. W. (1982) *Sulfatases of Microbial Origin*, Vol. 2, CRC Press, Inc., Boca Raton, FL.
13. Murooka, Y., Ishibashi, K., Yasumoto, M., Sasaki, M., Sugino, H., Azakami, H., and Yamashita, M. (1990) A sulfur- and tyramine-regulated *Klebsiella aerogenes* operon containing the arylsulfatase (atsA) gene and the atsB gene. *J. Bacteriol. 172*, 2131–2140.
14. Dierks, T., Schmidt, B., Borissenko, L. V., Peng, J., Preusser, A., Mariappan, M., and von Figura, K. (2003) Multiple sulfatase deficiency is caused by mutations in the gene encoding the human Cα-formylglycine generating enzyme. *Cell 113*, 435–444.
15. Cosma, M. P., Pepe, S., Annunziata, I., Newbold, R. F., Grompe, M., Parenti, G., and Ballabio, A. (2003) The multiple sulfatase deficiency gene encodes an essential and limiting factor for the activity of sulfatases. *Cell 113*, 445–456.
16. Berteau, O., Guillot, A., Benjdia, A., and Rabot, S. (2006) A new type of bacterial sulfatase reveals a novel maturation pathway in prokaryotes. *J. Biol. Chem. 281*, 22464–22470.
17. Dierks, T., Miech, C., Hummerjohann, J., Schmidt, B., Kertesz, M. A., and von Figura, K. (1998) Posttranslational formation of formylglycine in prokaryotic sulfatases by modification of either cysteine or serine. *J. Biol. Chem. 273*, 25560–25564.
18. Miech, C., Dierks, T., Selmer, T., von Figura, K., and Schmidt, B. (1998) Arylsulfatase from *Klebsiella pneumoniae* carries a formylglycine generated from a serine. *J. Biol. Chem. 273*, 4835–4837.
19. Lukatela, G., Krauss, N., Theis, K., Selmer, T., Gieselmann, V., von Figura, K., and Saenger, W. (1998) Crystal structure of human arylsulfatase A: The aldehyde function and the metal ion at the active site suggest a novel mechanism for sulfate ester hydrolysis. *Biochemistry 37*, 3654–3664.
20. Recksiek, M., Selmer, T., Dierks, T., Schmidt, B., and von Figura, K. (1998) Sulfatases, trapping of the sulfated enzyme intermediate by substituting the active site formylglycine. *J. Biol. Chem. 273*, 6096–6103.
21. Szameit, C., Miech, C., Balleininger, M., Schmidt, B., von Figura, K., and Dierks, T. (1999) The iron sulfur protein AtsB is required for posttranslational formation of formylglycine in the *Klebsiella* sulfatase. *J. Biol. Chem. 274*, 15375–15381.
22. Marquordt, C., Fang, Q. H., Will, E., Peng, J. H., von Figura, K., and Dierks, T. (2003) Posttranslational modification of serine to formylglycine in bacterial sulfatases: Recognition of the modification motif by the iron-sulfur protein AtsB. *J. Biol. Chem. 278*, 2212–2218.
23. Fang, Q., Peng, J., and Dierks, T. (2004) Post-translational formylglycine modification of bacterial sulfatases by the radical S-adenosylmethionine protein AtsB. *J. Biol. Chem. 279*, 14570–14578.
24. The_UniProt_Consortium (2007) The Universal Protein Resource (UniProt). *Nucleic Acids Res. 35*, D193–D197.
25. Sofia, H. J., Chen, G., Hetzler, B. G., Reyes-Spindola, J. F., and Miller, N. E. (2001) Radical SAM, a novel protein superfamily linking unresolved steps in familiar biosynthetic pathways with radical mechanisms: Functional characterization using new analysis and information visualization methods. *Nucleic Acids Res. 29*, 1097–1106.
26. Layer, G., Heinz, D. W., Jahn, D., and Schubert, W. D. (2004) Structure and function of radical SAM enzymes. *Curr. Opin. Chem. Biol. 8*, 468–476.
27. Frey, P. A., Hegeman, A. D., and Reed, G. H. (2006) Free radical mechanisms in enzymology. *Chem. Rev. 106*, 3302–3316.
28. Fontecave, M., Mulliez, E., and Ollagnier-de Choudens, S. (2001) Adenosylmethionine as a source of 5′-deoxyadenosyl radicals. *Curr. Opin. Chem. Biol. 5*, 506–511.
29. Cheek, J., and Broderick, J. B. (2001) Adenosylmethionine-dependent iron-sulfur enzymes: Versatile clusters in a radical new role. *J. Biol. Inorg. Chem. 6*, 209–226.
30. Lepore, B. W., Ruzicka, F. J., Frey, P. A., and Ringe, D. (2005) The X-ray crystal structure of lysine-2,3-aminomutase from *Clostridium subterminale*. *Proc. Natl. Acad. Sci. U.S.A. 102*, 13819–13824.
31. Layer, G., Moser, J., Heinz, D. W., Jahn, D., and Schubert, W. D. (2003) Crystal structure of coproporphyrinogen III oxidase reveals cofactor geometry of radical SAM enzymes. *EMBO J. 22*, 6214–6224.
32. Hänzelmann, P., and Schindelin, H. (2004) Crystal structure of the S-adenosylmethionine-dependent enzyme MoaA and its implications for molybdenum cofactor deficiency in humans. *Proc. Natl. Acad. Sci. U.S.A. 101*, 12870–12875.
33. Berkovitch, F., Nicolet, Y., Wan, J. T., Jarrett, J. T., and Drennan, C. L. (2004) Crystal structure of biotin synthase, an S-adenosylmethionine-dependent radical enzyme. *Science 303*, 76–79.
34. Walsby, C. J., Ortillo, D., Broderick, W. E., Broderick, J. B., and Hoffman, B. M. (2002) An anchoring role for FeS clusters: Chelation of the amino acid moiety of S-adenosylmethionine to the unique iron site of the [4Fe−4S] cluster of pyruvate formate−lyase activating enzyme. *J. Am. Chem. Soc. 124*, 11270–11271.
35. Walsby, C. J., Hong, W., Broderick, W. E., Cheek, J., Ortillo, D., Broderick, J. B., and Hoffman, B. M. (2002) Electron-nuclear double resonance spectroscopic evidence that S-adenosylmethionine binds in contact with the catalytically active $[4Fe\text{-}4S]^{+}$ cluster of pyruvate formate-lyase activating enzyme. *J. Am. Chem. Soc. 124*, 3143–3151.
36. Krebs, C., Broderick, W. E., Henshaw, T. F., Broderick, J. B., and Huynh, B. H. (2002) Coordination of adenosylmethionine to a unique iron site of the [4Fe-4S] of pyruvate formate−lyase activating enzyme: A Mössbauer spectroscopic study. *J. Am. Chem. Soc. 124*, 912–913.
37. Chen, D., Walsby, C., Hoffman, B. M., and Frey, P. A. (2003) Coordination and mechanism of reversible cleavage of S-adenosylmethionine by the [4Fe-4S] center in lysine 2,3-aminomutase. *J. Am. Chem. Soc. 125*, 11788–11789.
38. Iwig, D. F., and Booker, S. J. (2004) Insight into the polar reactivity of the onium chalcogen analogues of S-adenosyl-L-methionine. *Biochemistry 43*, 13496–13509.
39. Kennedy, M. C., Kent, T. A., Emptage, M., Merkle, H., Beinert, H., and Münck, E. (1984) Evidence for the formation of a linear [3Fe-4S] cluster in partially unfolded aconitase. *J. Biol. Chem. 259*, 14463–14471.
40. Beinert, H. (1983) Semi-micro methods for analysis of labile sulfide and of labile sulfide plus sulfane sulfur in unusually stable iron-sulfur proteins. *Anal. Biochem. 131*, 373–378.
41. Beinert, H. (1978) Micro methods for the quantitative determination of iron and copper in biological material. *Methods Enzymol. 54*, 435–445.
42. Cicchillo, R. M., Lee, K. H., Baleanu-Gogonea, C., Nesbitt, N. M., Krebs, C., and Booker, S. J. (2004) *Escherichia coli* lipoyl synthase binds two distinct [4Fe-4S] clusters per polypeptide. *Biochemistry 43*, 11770–11781.

43. Sambrook, J., Fritsch, E. F., and Maniatis, T. (1989) *Molecular Cloning: A Laboratory Manual*, 2nd ed., Vol. 3, Cold Spring Harbor Laboratory Press, Plainview, NY.
44. Ramamurthy, V., Swann, S. L., Paulson, J. L., Spedaliere, C. J., and Mueller, E. G. (1999) Critical aspartic acid residues in pseudouridine synthases. *J. Biol. Chem. 274*, 22225–22230.
45. Bradford, M. (1976) A rapid and sensitive method for the quantitation of microgram quantities of protein utilizing the principle of protein dye-binding. *Anal. Biochem. 72*, 248–254.
46. Benjdia, A., Leprince, J., Guillot, A., Vaudry, H., Rabot, S., and Berteau, O. (2007) Anaerobic sulfatase-maturating enzymes: Radical SAM enzymes able to catalyze in vitro sulfatase post-translational modification. *J. Am. Chem. Soc. 129*, 3462.
47. Cicchillo, R. M., Iwig, D. F., Jones, A. D., Nesbitt, N. M., Baleanu-Gogonea, C., Souder, M. G., Tu, L., and Booker, S. J. (2004) Lipoyl synthase requires two equivalents of S-adenosyl-L-methionine to synthesize one equivalent of lipoic acid. *Biochemistry 43*, 6378–6386.
48. Johnson, D., Unciuleac, M., and Dean, D. R. (2006) Controlled expression and functional analysis of iron-sulfur cluster biosynthetic components within *Azotobacter vinelandii*. *J. Bacteriol. 188*, 7551–7561.
49. Kent, T. A., Huynh, B. H., and Münck, E. (1980) Iron−sulfur proteins: Spin-coupling model for three-iron clusters. *Proc. Natl. Acad. Sci. U.S.A. 77*, 6574–6576.
50. Peng, J., Schmidt, B., von Figura, K., and Dierks, T. (2003) Identification of formylglycine in sulfatases by matrix-assisted laser desorption/ionization time-of-flight mass spectrometry. *J. Mass Spectrom. 38*, 80–86.
51. Booker, S. J., Cicchillo, R. M., and Grove, T. L. (2007) Self-sacrifice in radical S-adenosylmethionine proteins. *Curr. Opin. Chem. Biol. 11*, 543–552.
52. Jameson, G. N. L., Cosper, M. M., Hernández, H. L., Johnson, M. K., and Huynh, B. H. (2004) Role of the [2Fe-2S] cluster in recombinant *Escherichia coli* biotin synthase. *Biochemistry 43*, 2022–2031.
53. Tse Sum Bui, B., Benda, R., Schünemann, V., Florentin, D., Trautwein, A. X., and Marquet, A. (2003) Fate of the $[2Fe\text{-}2S]^{2+}$ cluster of *Escherichia coli* biotin synthase during reaction: A Mössbauer characterization. *Biochemistry 42*, 8791–8798.
54. Ugulava, N. B., Sacanell, C. J., and Jarrett, J. T. (2001) Spectroscopic changes during a single turnover of biotin synthase: Destruction of a [2Fe-2S] cluster accompanies sulfur insertion. *Biochemistry 40*, 8352–8358.
55. Pierrel, F., Douki, T., Fontecave, M., and Atta, M. (2004) MiaB protein is a bifunctional radical-S-adenosylmethionine enzyme involved in thiolation and methylation of tRNA. *J. Biol. Chem. 279*, 47555–47653.
56. Sancho, J. (2006) Flavodoxins: Sequence, folding, binding, function and beyond. *Cell. Mol. Life Sci. 63*, 855–864.
57. Mulliez, E., Padovani, D., Atta, M., Alcouffe, C., and Fontecave, M. (2001) Activation of class II ribonucleotide reductase by flavodoxin: A protein radical-driven electron transfer to the iron−sulfur center. *Biochemistry 40*, 3730–3736.
58. Birch, O. M., Fuhrmann, M., and Shaw, N. M. (1995) Biotin synthase from *Escherichia coli*, an investigation of the low molecular weight and protein components required for activity in vitro. *J. Biol. Chem. 270*, 19158–19165.
59. Knappe, J., and Schmitt, T. (1976) A novel reaction of S-adenosyl-L-methionine correlated with the activation of pyuvate formate−lyase. *Biochem. Biophys. Res. Commun. 71*, 1110–1117.
60. Hoover, D. M., Jarrett, J. T., Sands, R. H., Dunham, W. R., Ludwig, M. L., and Matthews, R. G. (1997) Interaction of *Escherichia coli* cobalamin-dependent methionine synthase and its physiological partner: Binding of flavodoxin leads to axial ligand dissociation from the cobalamin. *Biochemistry 36*, 127–138.
61. Frazzon, J., and Dean, D. R. (2003) Formation of iron−sulfur clusters in bacteria: An emerging field in bioinorganic chemistry. *Curr. Opin. Chem. Biol. 7*, 166–173.
62. Wang, S. C., and Frey, P. A. (2007) Binding energy in the one-electron reductive cleavage of S-adenosylmethionine in lysine 2,3-aminomutase, a radical SAM enzyme. *Biochemistry 46*, 12889–12895.
63. Ugulava, N. B., Gibney, B. R., and Jarrett, J. T. (2001) Biotin synthase contains two distinct iron−sulfur binding sites: Chemical and spectroelectrochemical analysis of iron−sulfur cluster interconversions. *Biochemistry 40*, 8343–8351.
64. Layer, G., Verfurth, K., Mahlitz, E., and Jahn, D. (2002) Oxygen-independent coproporphyrinogen-III oxidase HemN from *Escherichia coli*. *J. Biol. Chem. 277*, 34136–34142.
65. Beinert, H., Kennedy, M. C., and Stout, C. D. (1996) Aconitase as iron-sulfur protein, enzyme, and iron-regulatory protein. *Chem. Rev. 96*, 2335–2373.
66. Cicchillo, R. M., Baker, M. A., Schnitzer, E. J., Newman, E. B., Krebs, C., and Booker, S. J. (2004) *Escerhichia coli* L-serine deaminase requires a [4Fe-4S] cluster in catalysis. *J. Biol. Chem. 279*, 32418–32425.
67. Fling, D. H., and Allen, R. M. (1996) Iron−sulfur proteins with nonredox functions. *Chem. Rev. 96*, 2315–2334.
68. Lippard, S. J., and Berg, J. M. (1994) *Principles of Bioinorganic Chemistry*, University Science Books, Mill Valley, CA.
69. Golden, D. M., and Benson, S. W. (1969) Free-radical and molecule thermochemistry from studies of gas-phase iodine-atom reactions. *Chem. Rev. 69*, 125–134.
70. Steigerwald, M. L., Goddard, W. A., III, and Evans, D. A. (1979) Theoretical studies of the oxy anionic substituent effect. *J. Am. Chem. Soc. 101*, 1994–1997.
71. Cosper, M. M., Jameson, G. N. L., Hernández, H. L., Krebs, C., Huynh, B. H., and Johnson, M. K. (2004) Characterization of the cofactor composition of *Escherichia coli* biotin synthase. *Biochemistry 43*, 2007–2021.
72. Henry, D. J., Parkinson, C. J., Mayer, P. M., and Radom, L. (2001) Bond dissociation energies and radical stabilization energies associated with substituted methyl radicals. *J. Phys. Chem. A 105*, 6750–6756.
73. Benjdia, A., Subramanian, S., Leprince, J., Vaudry, H., Johnson, M. K., and Berteau, O. (2008) Anaerobic sulfatase-maturating enzymes: First dual substrate radical S-adenosylmethionine enzymes. *J. Biol. Chem. 283*, in press.
74. Jarrett, J. T. (2003) The generation of 5′-deoxyadenosyl radicals by adenosylmethionine-dependent radical enzymes. *Curr. Opin. Chem. Biol. 7*, 174–182.
75. Frey, P. A., and Magnusson, O. T. (2003) S-Adenosylmethionine: A wolf in sheep's clothing, or a rich man's adenosylcobalamin? *Chem. Rev. 103*, 2129–2148.
76. Frey, P. A., and Booker, S. J. (2001) Radical mechanisms of S-adenosylmethionine-dependent enzymes. *Adv. Protein Chem. 58*, 1–45.
77. Frey, P. A., and Booker, S. (1999) Radical intermediates in the reaction of lysine 2,3-aminomutase. In *Advances in Free Radical Chemistry* (Zard, S. Z., Ed.) pp 1−43, JAI Press Inc., Stamford, CT.
78. Ruzicka, F. J., and Frey, P. A. (2007) Glutamate 2,3-aminomutase: A new member of the radical SAM superfamily of enzymes. *Biochim. Biophys. Acta 1774*, 286–296.
79. Slieman, T. A., Rebeil, R., and Nicholson, W. L. (2000) Spore photoproduct (SP) lyase from *Bacillus subtilis* specifically binds to and cleaves SP (5-thyminyl-5,6-dihydrothymine) but not cyclobutane pyrimidine dimers in UV-irradiated DNA. *J. Bacteriol. 182*, 6412–6417.
80. Rebeil, R., and Nicholson, W. L. (2001) The subunit structure and catalytic mechanism of the *Bacillus subtilis* DNA repair enzyme spore photoproduct lyase. *Proc. Natl. Acad. Sci. U.S.A. 98*, 9038–9043.
81. Cheek, J., and Broderick, J. B. (2002) Direct H atom abstraction from spore photoproduct C-6 initiates DNA repair in the reaction catalyzed by spore photoproduct lyase: Evidence for a reversibly generated adenosyl radical intermediate. *J. Am. Chem. Soc. 124*, 2860–2861.
82. Buis, J. M., Cheek, J., Kalliri, E., and Broderick, J. B. (2006) Characterization of an active spore photoproduct lyase, a DNA repair enzyme in the radical S-adenosylmethionine superfamily. *J. Biol. Chem. 281*, 25994–26003.
83. Wagner, A. F., Frey, M., Neugebauer, F. A., Schäfer, W., and Knappe, J. (1992) The free radical in pyruvate formate-lyase is located on glycine-734. *Proc. Natl. Acad. Sci. U.S.A. 89*, 996–1000.
84. Knappe, J., and Wagner, A. F. (2001) Stable glycyl radical from pyruvate formate-lyase and ribonucleotide reductase (III). *Adv. Protein Chem. 58*, 277–315.
85. Jarrett, J. T. (2005) The novel structure and chemistry of iron-sulfur clusters in the adenosylmethionine-dependent radical enzyme biotin synthase. *Arch. Biochem. Biophys. 433*, 312–321.
86. Cicchillo, R. M., and Booker, S. J. (2005) Mechanistic investigations of lipoic acid biosynthesis in *Escherichia coli*: Both sulfur

atoms in lipoic acid are contributed by the same lipoyl synthase polypeptide. *J. Am. Chem. Soc. 127*, 2860–2861.
87. Hernández, H. L., Pierrel, F., Elleingand, E., García-Serres, R., Huynh, B. H., Johnson, M. K., Fontecave, M., and Atta, M. (2007) MiaB, a bifunctional radical-S-adenosylmethionine enzyme involved in the thiolation and methylation of tRNA, contains two essential [4Fe-4S] clusters. *Biochemistry 46*, 5140–5147.
88. Yokoyama, K., Numakura, M., Kudo, F., Ohmori, D., and Eguchi, T. (2007) Characterization and mechanistic study of a radical SAM dehydrogenase in the biosynthesis of butirosin. *J. Am. Chem. Soc. 129*, 15147–15155.

BI8004297